[American Journal of Science, Vol. 309, September, 2009, P. 517–548, DOI 10.2475/07.2009.01]

American Journal of Science

SEPTEMBER 2009

NUMERICAL SIMULATION OF KINETICALLY-CONTROLLED CALC-SILICATE REACTIONS AND FLUID FLOW WITH TRANSIENT PERMEABILITY AROUND CRYSTALLIZING PLUTONS

PETER I. NABELEK

Department of Geological Sciences, University of Missouri, Columbia, Missouri 65211, USA; nabelekp@missouri.edu

ABSTRACT. Numerical simulations were performed to examine the relationships between variable contact-aureole permeability, the kinetics of calc-silicate reactions, and the fluxes of mixed CO_2-H_2O fluids around a crystallizing granite laccolith. The role of magmatic water was explicitly considered. The Notch Peak contact-metamorphic aureole in Utah was used to define the stratigraphy of the model domain and rock compositions. Reactions that were considered include the major isograd-defining reactions that occurred in the Notch Peak aureole. The half-space model domain had the laccolith, 2 km thick at the middle apex. Only 1-phase fluid flow was considered.

Results show that the evolution of the fluid flow-field is highly dependent on the pressure (*P*) boundary condition at the top of the model domain. When *P* at the top boundary is allowed to increase, *P* in most of the top half of the domain eventually exceeds the lithostatic pressure plus the assumed tensile strength of rocks of 15 MPa. This boundary condition simulates an unvented flow-system. A more realistic boundary condition, one that simulates a system that is able to vent to the surface, is when *P* at the top boundary is held at a hydrostatic pressure. In this case, the flow-field is determined largely by pressure gradients between the overpressured magmatic fluid exsolving from the pluton and the lower pressures at the domain boundaries. Fracturing is predicted to occur early after pluton emplacement as the pore fluid is heated and metamorphic reactions produce CO_2. Although fracturing and reaction-enhanced porosity and permeability influence the local flow-field, the domain-scale flow-field is controlled by long-distance pressure gradients. The domain-scale flow-field and temperature distribution impose the largest control on the distribution of major mineral assemblages in the metamorphic aureole. Transient changes in permeability due to fracturing and volume changes in the solid matrix that accompany reactions have a smaller control on the distribution of minerals.

The simulations predict significant overstepping and coeval progress of metamorphic reactions. Reaction rates range from 5×10^{-10} to 10^{-14} kmol/m^2/sec, depending on the actual *P-T-X*CO_2^f conditions and the abundance of the rate-controlling mineral. Throughout the metamorphic aureole, *X*CO_2^f approaches 1 as CO_2 evolved by reactions displaces H_2O. High pore pressures prevent magmatic H_2O from infiltrating the aureole until pressures drop when reactions are approaching completion. Consequently, only in the inner aureole, which is eventually infiltrated by magmatic H_2O, can minerals such as wollastonite and vesuvianite be produced. An integrated H_2O flux of 3×10^4 kmol/m^2 is required to produce the width of the model wollastonite zone by 20 ky. Because of pressure gradients, CO_2 that is produced in the inner aureole flows outward into colder rocks even before these rocks are heated. The *T-X*CO_2^f paths in outer aureole rocks cut across the H_2O-CO_2 solvus, which predicts that in nature H_2O and CO_2 should unmix and behave as two separate fluid phases. The average yearly CO_2 flux at the top of the model domain, 2.3×10^3 mol/m^2/y, is comparable to fluxes of metamorphic carbonic fluids in active geothermal fields.

INTRODUCTION

The major consequences of magma intrusion into the upper crust are the generation of convective fluid systems and metamorphism of wall rocks. Fluids that contribute to the flow systems include pore-fluids from the aureole rocks, magmatic fluids, and fluids generated by metamorphic reactions. Meteoric water may also invade magmatic-hydrothermal systems in shallow parts of the crust. Intrusion-induced fluid-flow systems contribute to heat and mass-transport in the crust, including the generation of ore deposits and geothermal systems. Because mineral reactions in contact aureoles are directly related to fluid flow and compositional properties of flow systems (Greenwood, 1975; Baumgartner and Ferry, 1991; Ferry, 1991), metamorphic petrologists have had good success in deducing the general properties of fossil intrusion-related fluid-flow systems from studies of mineral assemblages, but have had difficulty in deducing how the systems evolve over time.

Issues related to coupled metamorphic reactions with fluid flow that have been previously discussed in published works but are difficult to access from field-based studies alone, include 1) the relationship between fluid infiltration, reaction progress, and transient permeability variations, often referred to as "reaction-enhanced permeability", 2) the relationship between fluid production and fracturing of rocks, and 3) the effect of kinetic retardation on progress of metamorphic reactions and fluid production. The evidence for reaction-enhanced permeability comes from the often observed positive relationship between the amount of reaction progress and the degree of isotopic exchange seen in high-grade portions of calc-silicate contact aureoles (Rumble and others, 1982; Nabelek and others, 1992; Nabelek, 2002). Calc-silicates typically show substantial isotopic exchange, whereas marbles derived from silicate-poor limestones or dolostones show little isotopic exchange because the potential for reaction progress is greater in polymineralic rocks than in rocks dominated by one mineral. In the field, reaction-enhanced permeability is suggested by deformation related to volume reduction in the mineralogy of calc-silicates. For example, the volume reduction during the stoichiometric production of wollastonite from quartz + calcite is 33 percent. Reaction-enhanced permeability may influence the fluid flow-field because the highest fluid flux will be focused to zones with the highest permeability. Indeed, the largest shifts in isotopic compositions of rocks and minerals typically occur in inner aureoles where the largest changes in the volumes of solids occur (Nabelek and Labotka, 1993; Bowman and others, 1994; Roselle and others, 1999; Nabelek, 2002). Because reaction-enhanced permeability is transient, it may influence evolution of the fluid flow-field differently compared to a homogeneous permeability structure or compared to a heterogeneous but time-invariable permeability structure of an aureole (Cathless, 1981; Norton, 1984; Gerdes and others, 1998; Cui and others, 2001). Numerical simulations can reproduce broad isotopic and mineralogical features of aureoles if it is assumed, for example, that parts of aureoles that have undergone chemical and mineralogical alteration were inherently more permeable than parts that have experienced little alteration (Cook and others, 1997; Balashov and Yardley, 1998; Balashov and others, 1999; Cui and others, 2002, 2003). However, large differences in permeability among rock types may not be inherent to the deep crust (Manning and Ingebritsen, 1999), and therefore such models may not accurately represent the actual flow-fields around intrusions. If a high-permeability zone develops in the high-grade portion of an aureole, the dominant flow direction may become contact-parallel and produce reaction and chemical alteration steps that parallel the flow direction instead of being reaction fronts that are perpendicular to it (Yardley and Lloyd, 1995; Nabelek, 2002; Ague, 2003).

It is apparent from many metamorphic environments, including contact aureoles, that pore-pressure increase during heating of rocks and local fluid production

produces fractures that serve as conduits for fluid flow (Oliver and others 1983; Yardley, 1986; Manning and Bird, 1991; Ague, 1995; Nabelek, 2002). Fluid pressures may fluctuate during a metamorphic event when fractures open or are sealed by newly-formed minerals, when the solid assemblage looses volume, or when fluid production is episodic, either related to transient fluid exsolution out of the causative pluton or to onsets of metamorphic reactions (Dutrow and Norton, 1995; Balashov and Yardley, 1998; Labotka and others, 2002).

The relationship between reactive fluid flow and metamorphic reactions can also be influenced by the kinetics of metamorphic reactions (Müller and others, 2009). In contact aureoles, where rapid changes in temperature and fluid pressure occur, the onsets of reactions and consumption of reactant minerals can be significantly overstepped (Lasaga and Rye, 1993; Lasaga and others, 2000; Bolton and others, 2004; Lüttge and others, 2004; Nabelek, 2007). The consequence of retarded consumption of reactant minerals is that several reactions may be coeval, and in calc-silicates the continuous production of CO_2 may keep the local fluid pressure elevated, which in turn may prevent efficient influx of an external fluid. Kinetic effects may result in rocks in which reactant and product minerals coexist, giving apparent univariant assemblages (Hover-Granath and others, 1983), or in rocks in which high-temperature minerals were produced directly from metastable protolith minerals instead of intermediate products (Müller and others, 2004).

In this study, numerical simulations were performed to examine the relationships between variable contact-aureole permeability, the kinetics of calc-silicate reactions, and the fluxes of mixed CO_2-H_2O fluids around a crystallizing pluton. The role of magmatic water was explicitly considered. The numerical simulations provide images of a temporal evolution of fluid-flow systems around plutons that are difficult to discern empirically from mineral assemblages, which are the products of integrated temperature-pressure-$X\mathrm{CO}_2^{\mathrm{f}}$-time ($T$-$P$-$X\mathrm{CO}_2^{\mathrm{f}}$-$t$) paths in rocks.

MODEL SETUP

The numerical simulations were done in two dimensions using the U. S. Geological Survey, hybrid finite-element and finite-difference computer code SUTRA (Voss, 1984; Voss and Provost, 2002). The Fortran code was initially modified by Cui and others (2003) to include calculation of metamorphic reactions at elevated P and T conditions in the presence of mixed CO_2-H_2O fluids. Changes to the program code since then were directed toward improvement of its stability, ability to model transient permeability conditions, realistic treatment of fluid exsolution from a pluton, and improvements to the user interface. In addition, the code was parallelized so that a 40 ky simulation with 1 y time-steps can be completed in ~12 hrs. on an 8-core Macintosh computer.

The half-space model domain for the presented simulations was 10 km wide and 8 km deep with rectangular grid-spacing of 50 m (fig. 1). A half-laccolith, 3 km wide at the base and 2 km tall at the center, was located at the left side of the domain. The laccolithic shape and the size of the pluton are typical of many granitic plutons, including that of the Jurassic Notch Peak pluton in western Utah. The Notch Peak pluton and its contact aureole served as the model for the simulations. The structure of the model aureole approximates the Cambrian and Ordovician stratigraphy around the Notch Peak pluton (Hintze, 1974). The stratigraphy includes the Prospect Mountain quartzite at the bottom that is overlain by interbedded limestones and calcareous shales, now metamorphosed to marbles and calc-silicates, respectively, in the aureole. The most prominent of these calcareous formations are the Wheeler, Marjum, Weeks, and Orr Formations. The limestones and shales in these formations are interbedded at various thicknesses but in the simulations they were made to be of equal thickness. The limestones were assumed to be unreactive as is suggested by their unshifted oxygen and

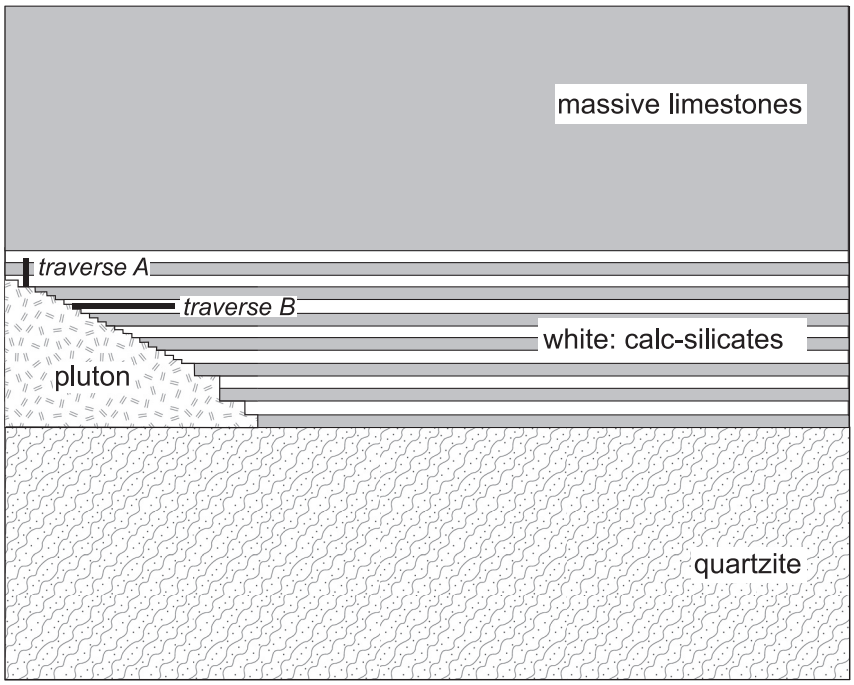

Fig. 1. Model domain used in numerical simulations. The domain is 8 km high and 10 km wide. The top of the domain is at 3 km depth. The simplified stratigraphy is based on the stratigraphy of wall-rocks around the Notch Peak intrusion in Utah. In the simulations, only calc-silicates were reactive and the pluton was a source of H_2O. Metamorphism of wollastonite, diopside, and tremolite-grade nodes at traverses A and B is described in the text.

carbon isotope ratios and mineral assemblages that are inconsistent with penetration of H_2O into the limestones (Hover-Granath and others, 1983; Nabelek and others, 1984; Nabelek, 2002). All metamorphic reactions were assumed to occur only in the calcareous shales. Above the calc-silicate subdomain is a thick sequence of mostly massive limestones that was also assumed to be unreactive.

The governing equation for heat transport in the simulations was (symbols in table 1):

$$\partial \frac{(\rho_m c_m T)}{\partial t} = -\nabla \cdot (\vec{u} \rho_f c_f \nabla T) + \nabla \cdot (K_m \nabla T) + Q. \tag{1}$$

The first term on the right-hand side describes the advective component, the second term the diffusive component, and the third term the local sources. Local sources for heat include heat of crystallization in the pluton (positive) and metamorphic reactions (negative). The conductivities used were 2.25 W/m/K for mineral assemblage and 0.6 W/m/K for fluid. The governing equations for mass transport, following Balashov and Yardley (1998), considered each fluid component separately:

$$\frac{\partial(\phi C_{H_2O})}{\partial t} = -\nabla \cdot (C_{H_2O} \vec{u}) + \nabla \cdot \left(\phi D \frac{\bar{\rho}_{CO_2}}{\rho_f} \nabla C_{H_2O} \right) + \Gamma_{H_2O} \tag{2a}$$

$$\frac{\partial(\phi C_{CO_2})}{\partial t} = -\nabla \cdot (C_{CO_2} \vec{u}) + \nabla \cdot \left(\phi D \frac{\bar{\rho}_{H_2O}}{\rho_f} \nabla C_{H_2O} \right) + \Gamma_{CO_2}. \tag{2b}$$

TABLE 1

Symbols used in equations

A	reactive surface area of grain
c_m	specific heat of rock or magma
c_f	specific heat of fluid
C_j	molar concentration of fluid component j
G	Gibbs free energy
D	interdiffusivity of H_2O and CO_2
$\vec{g}$	gravitational acceleration vector
k	permeability
K_m	thermal conductivity
P	pressure
Q	local heat source or sink
r'	reaction rate constant
R	reaction rate
t	time
T	temperature
ts	tensile strength of rocks
$\vec{u}$	fluid velocity vector
$X\mathrm{CO}_2^{\mathrm{f}}$	molar fraction of CO_2 in fluid
α	exponent in porosity-permeability relationship
ϕ	porosity
Γ_j	local source of fluid component j
ρ_m	density of rock or magma
ρ_f	density of fluid
$\overline{\rho}_j$	partial density of component j in fluid
μ	fluid viscosity
ν	reaction order

This formulation permits consideration of interdiffusion of CO_2 and H_2O with the net diffusive mass flux equal to zero. D of 2×10^{-8} m^2/sec was used (Fuller and others, 1966). Porosity in the diffusive terms accounts for diffusion occurring only through pore space. Local sources for fluid include metamorphic reactions and magmatic fluid. The Darcy fluid velocity is given by:

$$\vec{u} = -\frac{k}{\mu}\nabla(P + \rho_f \vec{g}). \tag{3}$$

In the grid, permeabilities and the diffusivity were mapped to elements, whereas pressure (P), temperature (T), fluid composition ($X\mathrm{CO}_2^{\mathrm{f}}$), porosity, and rock mineralogy were mapped to nodes, which constitute corners of elements. Permeabilities and diffusivities were assumed to be isotropic given the lack of mineral foliation in typical high-level metamorphic aureoles. The initial distributions of P and T in the model domain are shown in figure 2. The top of the model domain was assumed to be at 3 km depth. Hydrostatic fluid pressure was assumed in the wall rocks. In some simulations the pressure at all boundaries was allowed to vary whereas in most simulations shown, it was held at the initial hydrostatic pressure at the top boundary. The former condition implies that none of the boundaries in the model domain allow the transfer of

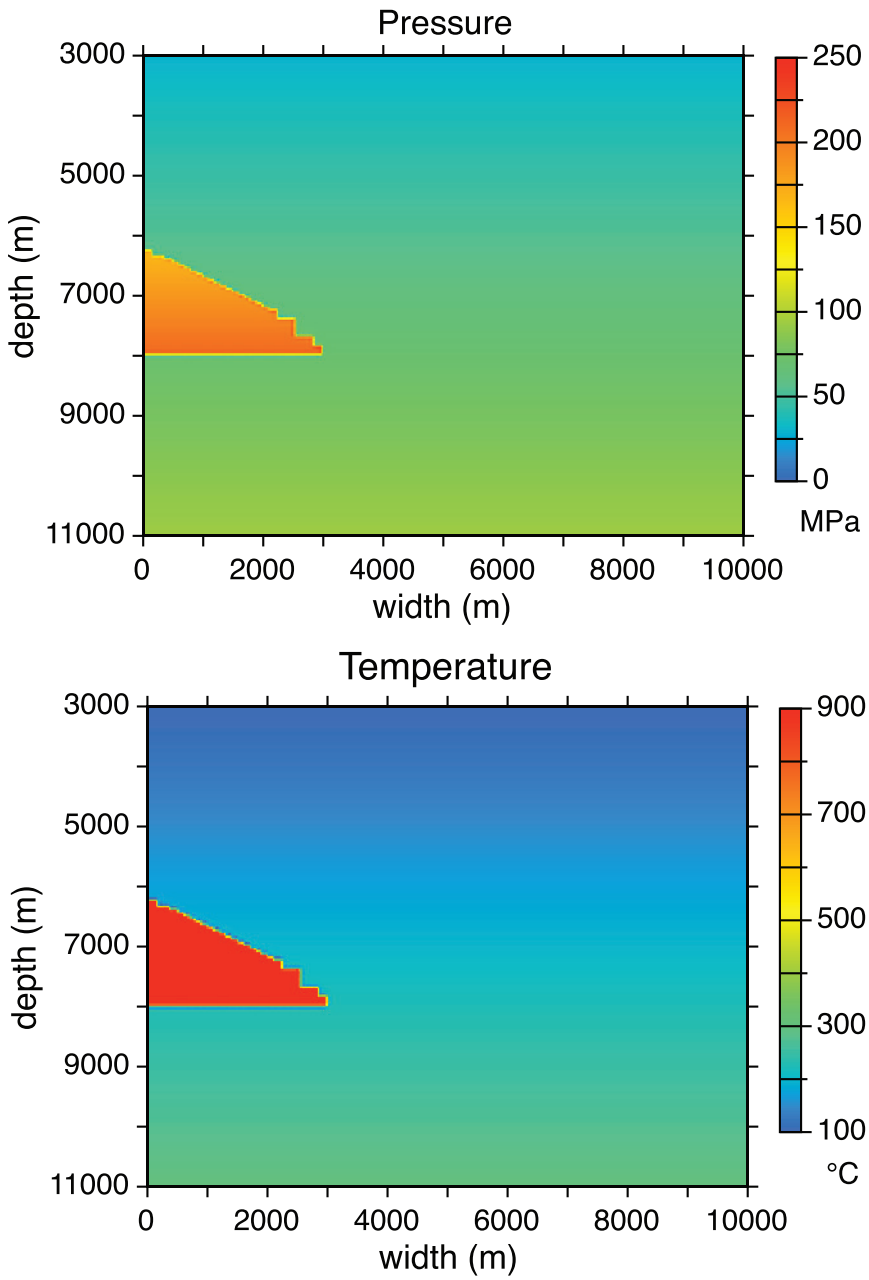

Fig. 2. Initial pressure and temperature conditions in the simulations. The laccolith is at lithostatic pressure before fluid exsolution begins. Fluid pressure in the wall-rocks is hydrostatic. The initial temperature in the laccolith is 900°C and in the wall-rocks is given by the geothermal gradient of 25°C/km.

pressure, whereas the latter condition implies pressure dissipation to overlying rocks. Temperature and XCO_2^f were allowed to vary at all boundaries. The initial magma temperature was 900 °C and the temperature in the wall rock domain was given by a 25°C geothermal gradient.

The fluid was assumed to be a CO_2-H_2O mixture without solutes. Fluid properties were calculated using the equation of state (EOS) of Holland and Powell (1991) as modified in Holland and Powell (1998). In this EOS the molar volumes of intermediate fluid compositions are linear mixtures of the molar volumes of pure CO_2 and H_2O, whereas direct measurements of mixed fluid properties give excess molar volumes for intermediate compositions (Sterner and Bodnar, 1991; Seitz and Blencoe, 1999; Blencoe and others, 1999). The EOS of Duan and Zhang (2006) encompasses this excess molar volume. Nevertheless, the EOS of Holland and Powell (1998) was chosen because it is internally consistent with the thermodynamic data for the modeled minerals. The initial XCO_2^f was assumed to be 0.03 in calcareous layers and 0.01 for the magmatic fluid and in the quartzite. The assumed low XCO_2^f in the aureole is based on the limited solubility of carbonate minerals in H_2O at elevated temperatures (Fein and Walther, 1987; Caciagli and Manning, 2003). The critical temperature for unmixing of a CO_2-H_2O fluid is ~270 °C with only a small dependence on pressures in the deep crust but with a strong dependence on salinity (fig. 3; Takenouchi and Kennedy, 1964; Bowers and Helgeson, 1983). At the low initial XCO_2^f, only one fluid phase is expected irrespective of salinity. However, during metamorphism, possible T-XCO_2^f-t paths may pass through the CO_2-H_2O immiscibility field, which may result in separation of carbonic and aqueous phases. Because the SUTRA code does not have a provision for modeling two-phase fluid flow, only a single mixed fluid phase was assumed to be always present. However, the modeling gives predictions in which part of a contact aureole fluid unmixing may occur. Some implications of potential fluid unmixing are discussed.

The initial concentration of H_2O in the magma was assumed to be 3 weight percent, which is approximately the minimum that can be in a granite melt generated by biotite-dehydration melting of a source at 900 °C and 10 kbar (Johannes and Holtz, 1996). Upon crystallization in the upper crust, at 1.5–2 kbar, H_2O begins to exsolve when magma is ~50 percent crystallized when the solubility limit of H_2O (~6 wt.%; Holtz and others, 1995) is reached. Assuming a linear decrease in the amount of melt with drop in temperature, the onset of water exsolution would begin at ~790 °C. H_2O was assumed to exsolve linearly from this temperature until the 680 °C solidus. In all simulations, the pluton had porosity of 0.003 and initial permeability of 10^{-19} m^2. The pressure in the pluton was initially lithostatic, but when a node reached 790 °C when H_2O exsolution began, pressure in the node was switched to hydrostatic and allowed to fluctuate and the proportional contribution of this node to permeabilities of the surrounding elements was increased to 10^{-18} m^2. In other words, the permeability of an element at each time step was determined by those properties of its surrounding nodes that triggered permeability changes (onset of H_2O exsolution for pluton nodes and change in porosity for aureole nodes; see below). The switch to hydrostatic pressure in the pluton permits the buildup of a high pressure in the portion of the pluton in which fluid exsolution is ongoing and, therefore, a more efficient escape of the fluid out of the pluton.

The modified SUTRA computer code uses the publicly-available Diagonally-Scaled BiConjugate Gradient (DSDBCG) sparse solver (Seager, 1989) to iteratively solve pressure, temperature, and fluid composition matrices because of their interdependence. The change in pressure for each time step in a node is solved from the change in the fluid mass resulting from density change and local fluid production. The initial relative convergence tolerances were 1×10^{-3} for pressure, 1×10^{-8} for temperature, and 1×10^{-4} for XCO_2. These tolerances were dynamically reduced during each simulation to account for smaller gradients, particularly in pressure, at later stages of simulations. The time-step for all simulations was 1 y.

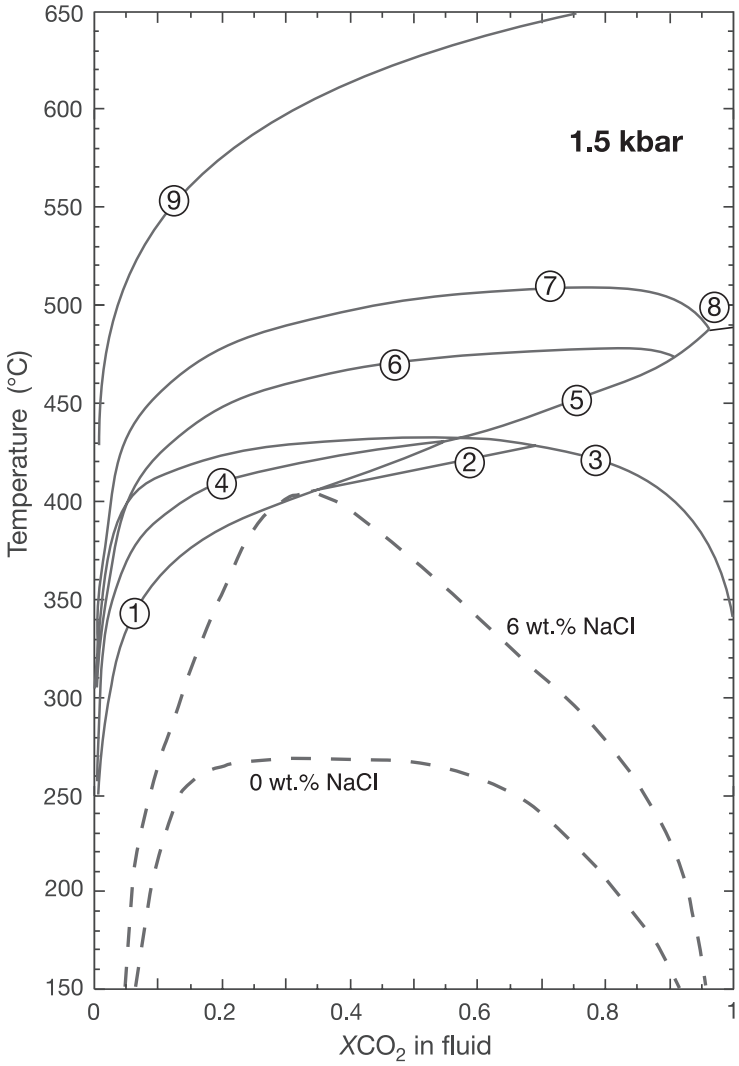

Fig. 3. Stable portions of calc-silicate reactions, in T-XCO_2^f space, that were used in the simulations. The numbers correspond to reactions in table 2. In the simulations, metastable extensions of the reactions were also used. The reactions in the figure were calculated for pressure of 1.5 kbar, although in the simulations the pressures in the nodes fluctuated. The dash lines show H_2O-CO_2 solvi for 0 and 6 wt.% NaCl (after Bowers and Helgeson, 1983).

Metamorphic Reactions

Metamorphic reactions that occurred in the Notch Peak calc-silicates are well described by the K-Ca-Mg-Al-Si-O-H-C (KCMASHC) system (table 2; fig. 3). Fe also occurs in the calc-silicates where its main effect is to reduce the stability fields of talc and tremolite (Nabelek, 2002). In fact, in the Notch Peak aureole talc occurs only in the marbles, which have high Mg/Fe ratios. The rate of reaction progress, R, is given by (Lasaga and Rye, 1993):

$$R = r' A \Delta G^v \qquad (4)$$

TABLE 2

Reactions used in modeling

1:	3 dol + 4 qtz + H_2O = 3 cc + tlc + 3 CO_2
2:	3 dol + ms + 2 qtz = phl + 2 cc + an + 4 CO_2
3:	ms + cc + 2 qtz = ksp + an + CO_2 + H_2O
4:	5 tlc + 6 cc + 4 qtz = 3 tr + 6CO_2 + 2 H_2O
5:	5 dol + 8 qtz + H_2O = tr + 3 cc + 7 CO_2
6:	5 phl + 6 cc + 24 qtz = 3 tr + 5 ksp + 6 CO_2 + 2 H_2O
7:	tr + 3 cc + 2 qtz = 5 di + 3 CO_2 + H_2O
8:	dol + 2 qtz = di + 2 CO_2
9:	cc + qtz = wo + CO_2

where r' is the reaction rate constant, A is the reactive surface area of minerals, ΔG is Gibbs free energy of reaction, and v is the reaction order. For all reactions, the reaction order v was assumed to be 1. The ΔG's of reactions were calculated using the thermodynamic data base and the EOS for CO_2-H_2O fluids of Holland and Powell (1998). The reaction rate constant was assumed to follow the Arrhenius rate law. Parameters were chosen to maximize the reaction rate, including the activation energy of 85 kJ/mol and the pre-exponential factor of 1×10^{-11} mol/m^2/sec/K (Lasaga and others, 2000). The reactive surface area was based on spherical grains 50 μm in diameter, and the rate was assumed to be dependent on the actual surface area of the least abundant mineral, calculated from the mineral's molar volume. These parameters were used for all reactions. The grain size is typical for unmetamorphosed and low-grade calc-silicate hornfelses in the Notch Peak aureole. A change in grain size with reaction progress was not considered because it is difficult to constrain. The initial mineralogy, in kmol/m^3, was assumed to be the average of calc-silicates in the Weeks Formation, 1.48 dolomite, 7.13 quartz, 19.42 calcite, and 0.22 muscovite. Not only the stable portions of reactions shown in figure 3 were used, but also the reactions' metastable extensions across the whole XCO_2^f range. Given the actual mineralogy of each node at a time step, the program chooses all reactions that have negative ΔG's at the actual T-P-XCO_2^f conditions. Only prograde reactions were allowed to occur, that is, only those reactions with products on the high-temperature sides of reaction boundaries. The progress of metamorphic reactions was solved using the subroutine ODE which integrates a system of ordinary differential equations over a time-step (Shampine and Gordon, 1975). The relative error tolerance was set to 1×10^{-4}.

Transient Porosity and Permeabilitity in the Aureole

In all simulations, initial permeability of 10^{-18} m^2 was assumed for all lithologies in the model aureole. This value is based on actual measurements on unmetamorphosed and high-grade calc-silicates in the Notch Peak aureole (Cui and others, 2001) and it is appropriate for most rocks in the deep crust (Manning and Ingebritsen, 1999). The porosity of deep-seated calc-silicate metamorphic rocks is thought to be 0.002–0.003, perhaps related to microcracks (Jamtveit and others, 1992). In the simulations, the initial porosity in the whole model domain was assumed to be 0.003. For the simulation of reaction-enhanced permeability, permeability was allowed to increase with porosity from the initial value of 10^{-18} m^2 according to the power-law relationship

$$k_n = k_i \left(\frac{\phi_n^\alpha}{\phi_i^\alpha} \right) \tag{5}$$

where i and n denote the initial and new permeability and porosity at each time step. α represents the sensitivity of the relationship and value of 2 was used in the simulations. This is a conservative value but appropriate for crystalline rocks in the deep crust (Walder and Nur, 1984). The increase in porosity was assumed to be directly related to the change in the molar volume of the mineral assemblage with reaction progress. The molar volume of the assemblage at each each node at each time-step was calculated from the molar volumes of the minerals and their actual proportions. For example, after the completion of diopside-forming reaction(s), the porosity became 0.07, and if the wollastonite-forming reaction went to completion, the porosity could potentially reach 0.135. Porosity of a node remained enhanced as long as pressure remained above lithostatic. If the pressure dropped below lithostatic, the node's porosity was reduced to the initial value. Because the permeability of each corner element depends on the porosity of all surrounding nodes, the permeability of each element was adjusted in proportion to the porosity change in each of its surrounding nodes. Porosity reduction due to creep (Balashov and Yardley, 1998) was not considered as creep is the function of strain rate, which is difficult to quantify in contact aureoles because among other factors it also depends on the rate at which magma is emplaced, and material flow properties, which are not well known for calc-silicates.

Given the small initial porosity, increases in temperature and decarbonation during reaction progress can result in fluid pressures that exceed lithostatic pressures. In nature, excess fluid pressures induce fractures in rocks. To simulate fracturing, when pressure in a given node exceeded lithostatic pressure plus the tensile strength of the rocks (ts), porosity increase in the node for the next time-step was assumed to be related to the amount of overpressure according to

$$\phi_n = \phi_i \left(\frac{P_{act}}{P_{lith}} \right) \tag{6}$$

where P_{act} is the actual fluid pressure and P_{lith} is the lithostatic pressure at the node. This relationship directly relates porosity increase by cracking to the molar volume of the heated pore fluid and generated fluid in the node. The tensile strength of the rocks was assumed to be 15 MPa, which is appropriate for carbonate and calc-silicate rocks (Lockner, 1995). The new porosity was then used to adjust the permeability of the surrounding elements using equation 5 for the next time-step. For brevity, only the term "permeability" is used to describe simulations with transient porosity and the dependent permeability, unless the term "porosity" is required by the context of the discussion.

RESULTS

Lithostatic Pressures and Fracturing

Figure 4 shows the dramatic effect of the top boundary pressure condition on the distribution of excess pressures ($P_{lith} + ts$) that are likely to occur around an intrusion. When pressure at the top boundary is allowed to increase, in other words, when there is no mechanism for pressure release, the area of excess pressure increases with time from small regions above and below the pluton to a region filling more than the top half of the aureole. The excess pressure comes from CO_2 production in the metamorphic domain, fluid exsolution from the pluton, and increase in molar volume of the pore fluid with temperature increase. The pressure in the domain is moderated by the assumed initial lithostatic pressure of the pluton until the pluton fully crystallizes at ~25 ky, at which point there is an unrealistic increase in excess pressure in the upper part of the model domain (fig. 5). Allowance for fracturing results in only a small reduction in excess pressures as the amount of introduced magmatic and metamor-

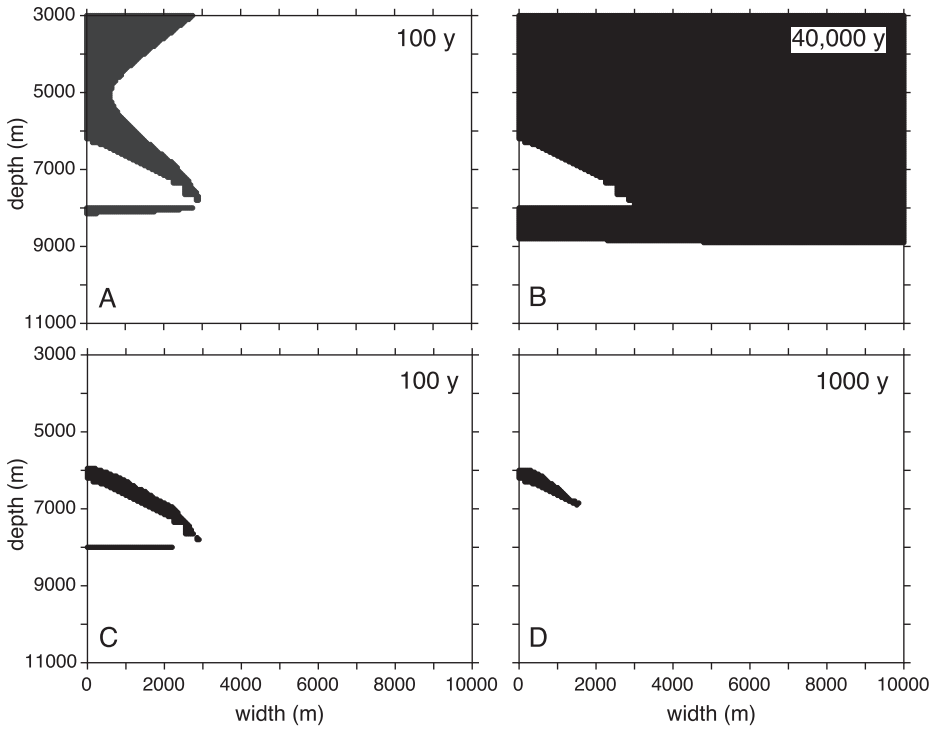

Fig. 4. Regions of the aureole domain (black) in which fluid pressure exceeds lithostatic at different times after intrusion of the magma. Parts (A) and (B) show overpressures when the pressure at the top boundary of the model domain is allowed to fluctuate. Parts (C) and (D) show overpressures when the pressure at the top boundary of the model domain is constrained to be hydrostatic. In this case, the pressure in the whole aureole domain drops below lithostatic by 10 ky.

phic fluid is not fully accommodated by the porosity increase. It is unlikely that in nature, high fluid overpressures throughout a large region around a pluton could be maintained without fracturing of overlying rocks and venting. Therefore, a boundary condition that does not simulate venting is thought to be unrealistic.

A more realistic size of overpressured region is obtained when the top boundary of the model domain is held at the initial hydrostatic pressure throughout a simulation. This boundary condition simulates venting of the fluid flow-system to the surface through overlying rocks or into an overlying groundwater system. Pressures remain in excess of lithostatic in both reactive and unreactive rocks only during the first few thousands of years and only within few hundreds of meters from the pluton (fig. 4). $P_{lith} + ts$ conditions are exceeded in reactive rocks only during the first ~140 yrs. after pluton emplacement, but can reoccur after reaction-enhanced porosity collapses (see below). The model fractured region would probably be somewhat more extensive and last longer with application of an EOS which expresses the positive excess volume for a mixed H_2O-CO_2 fluid (Blencoe and others, 1999; Duan and Zhang, 2006) instead of the EOS of Holland and Powell (1991, 1998). The hydrostatic pressure at the top boundary moderates the fluid pressures in the aureole and after crystallization of the whole pluton serves to eventually reduce pressures throughout the domain to hydrostatic (fig. 5). Allowance for fracturing changes somewhat the distribution of excess pressures with time, but there is little consequence on the evolution of the overall flow-system because it is mostly controlled by long-distance pressure gradients across

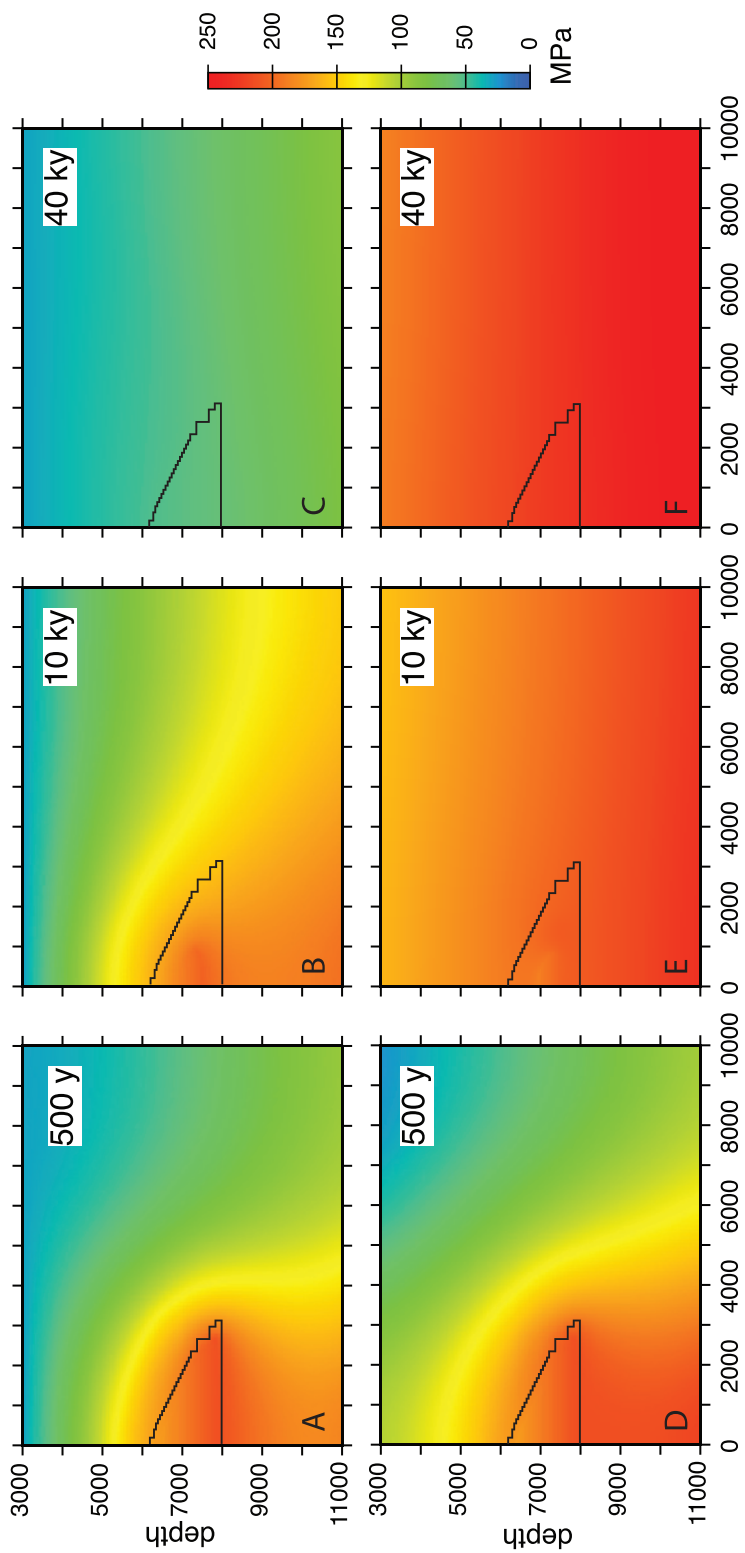

Fig. 5. The pressure field at three times after beginning of simulations. Parts (A-C) are for simulations with pressure at the top boundary constrained to be hydrostatic. Parts (D-F) are for simulations with pressure at the top boundary allowed to fluctuate. By the end of simulations at 40 ky, in the first case, the pressures drop to hydrostatic. The highest pressures are in that part of the pluton (outlined) in which H_2O exsolution is ongoing. In the second case, the pressures climb to greater than lithostatic in most of the model domain (fig. 4) because of the addition of magmatic and metamorphic fluids to the domain.

the model domain. In nature, where fluid pressures above plutons probably fluctuate between hydrostatic and lithostatic, models with unconstrained top boundary pressure suggest that fractures should develop directly above plutons. The difference between models with the two boundary conditions suggest that the extent of fracturing will depend on how efficiently the fluid system is vented. However, because the fixed top boundary pressure implies venting of the system, further discussion will be focused on models with this boundary condition.

P-T-XCO_2^f-t Paths and Reaction Kinetics

Pressure-temperature-XCO_2^f-time paths in the model aureole are complex. They depend on the kinetics of decarbonation reactions and fluid inflows, in addition to temperature changes. Figure 6 shows *T*-XCO_2^f-*t* paths for three nodes above the pluton (traverse A in fig. 1) and three nodes along the sloping side (traverse B in fig. 1). These paths were calculated without accounting for transient permeability changes. Figure 7 shows *T*-XCO_2^f-*t* paths for the same nodes, but these paths were calculated with account for reaction-enhanced permeability. Paths calculated with simulated fracturing are not significantly different and therefore are not shown.

In all model rocks, fluid composition at some stage becomes pure or nearly pure CO_2, either from local decarbonation reactions or because of CO_2 influx from rocks undergoing decarbonation upstream. In rocks near the contact, in the eventual wollastonite zone, CO_2 is initially mostly locally generated and it rapidly replaces H_2O in the pores. The *T*-XCO_2^f-*t* paths are initially internally buffered by the reactions because the onset of decarbonation reactions precedes the onset of exsolution of H_2O from the pluton. Reaction rates are typically 10^{-13} to 5×10^{-10} kmol/m^2/sec. Rapid heating leads to multiple overlapping reactions because reactants are not completely consumed by the first encountered reactions that should cause their disappearance (fig. 8). For example, in the wollastonite zone of traverse B in the model with reaction-enhanced permeability, dolomite is not completely consumed by the talc-forming reaction (1). Instead, dolomite is also involved in the initial production of tremolite by reaction (5) on the low-XCO_2 side, production of phlogopite by reaction (2), production of tremolite again by reaction (5) on the high-XCO_2 side, and finally it is consumed by both overstepped reaction (5) and the diopside-forming reaction (8). Figure 8 shows that near the contact where temperature is rapidly rising, multiple reactions are concurrent. Once the rate of CO_2 production diminishes in a given node and its neighbors, magmatic H_2O can infiltrate the inner aureole and result in the eventual production of wollastonite by reaction (9).

In the case with no reaction-enhanced permeability, fluid composition fluctuates more than with reaction-enhanced permeability prior to reaching reaction (9) (compare figs. 6 and 7), partly because the composition of a fluid occupying a larger pore space is less sensitive to infiltration of fluid from the outside and partly because the higher permeability zone serves as a mixing zone for fluids coming from neighboring nodes. The higher porosity and permeability moderate pressure fluctuations (fig. 9). A portion of wollastonite forms while fluid composition is buffered by reaction (9), either during heating or cooling, when the rate of H_2O infiltration is smaller than the rate of wollastonite production. However, additional wollastonite forms on the H_2O-side of reaction (9) when the rate of H_2O infiltration exceeds the rate of the reaction as quartz progressively disappears. Quartz finally disappears on the H_2O side of the *T*-XCO_2^f space. The final mineral assemblage contains wollastonite, diopside, and calcite, which agrees with the observed assemblage in the Notch Peak aureole. Vesuvianite is also common in the Weeks Formation of the Notch Peak aureole. The formation of vesuvianite requires nearly pure H_2O, which is generated here by the simulation.

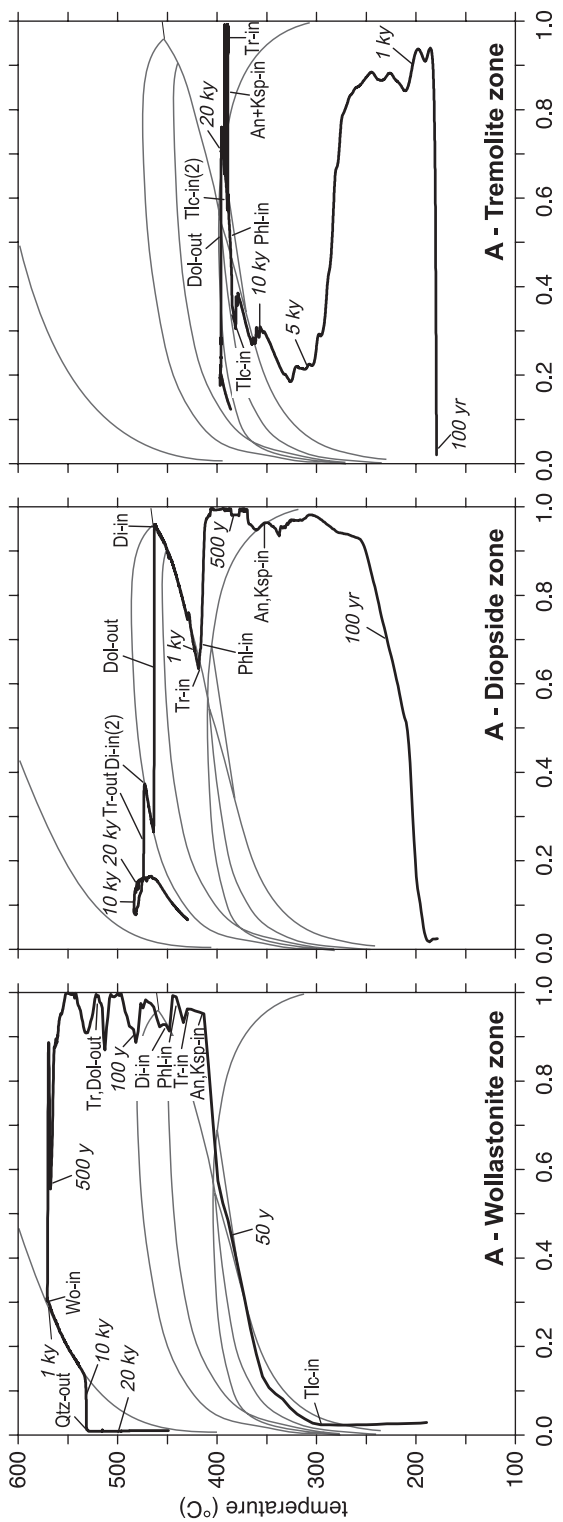

Fig. 6. Simulated T-XCO_2^f-t paths at traverses A and B shown in figure 1. These paths are for a model without account for transient permeability changes. Paths for selected nodes in wollastonite, diopside, and tremolite zones are shown for both traverses. The wollastonite nodes are next to the pluton, whereas the diopside and tremolite nodes are in the middle of their respective zones. Thin lines are metamorphic reactions shown in figure 3. The paths are marked by appearances and disappearances of selected minerals and by times in years. Because the model reactions are polybaric and the prevalent pressure varies across the aureole, the temperatures of the reactions were shifted to correspond to the prevalent pressure in each illustrated node. T-XCO_2^f-t paths in all nodes show a shift in XCO_2^f to high values and then a decrease. In the wollastonite zone, XCO_2^f fluctuates in response to inflows from surrounding nodes prior to growth of wollastonite along reaction (9). In the tremolite zone, XCO_2^f fluctuates several times near the peak temperature.

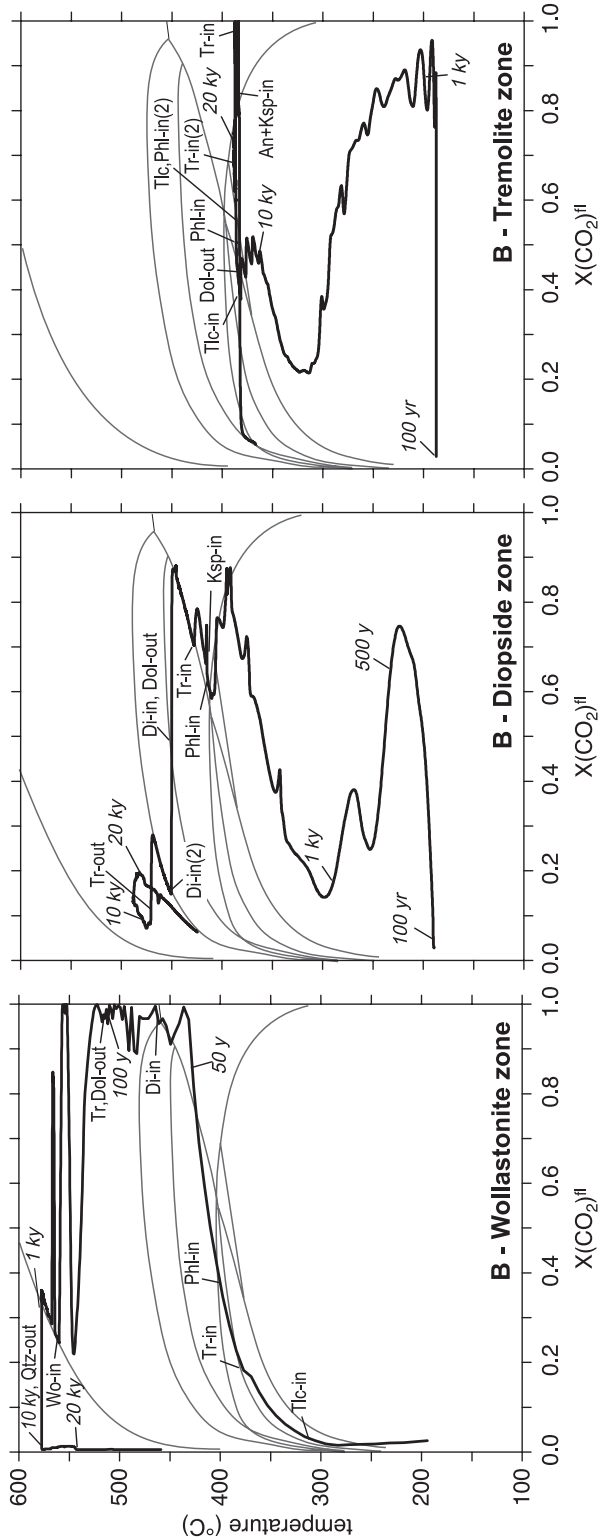

Fig. 6 (continued).

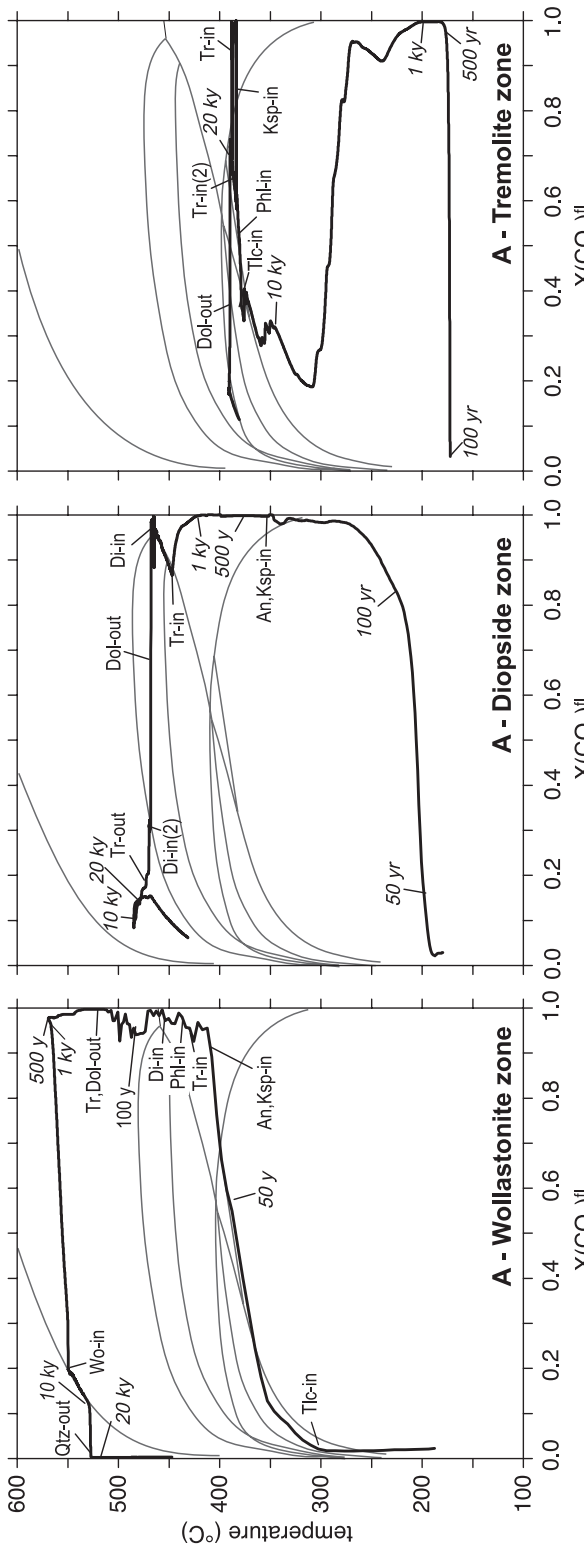

Fig. 7. Simulated T-XCO_2^f-t paths for a model with reaction-enhanced permeability. See figure 6 for explanation of labels in this figure. In comparison with a model without reaction-enhanced permeability (fig. 6), there is less fluctuation in XCO_2^f in wollastonite and diopside zones.

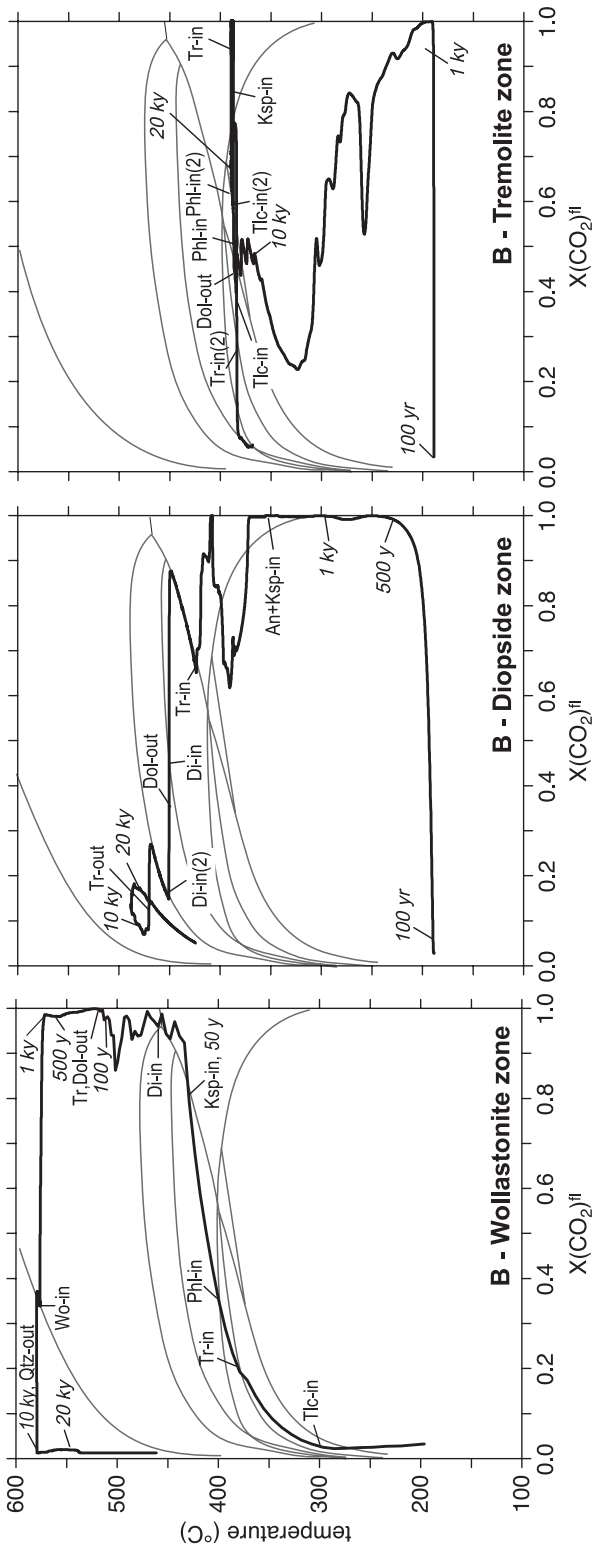

Fig. 7 (continued).

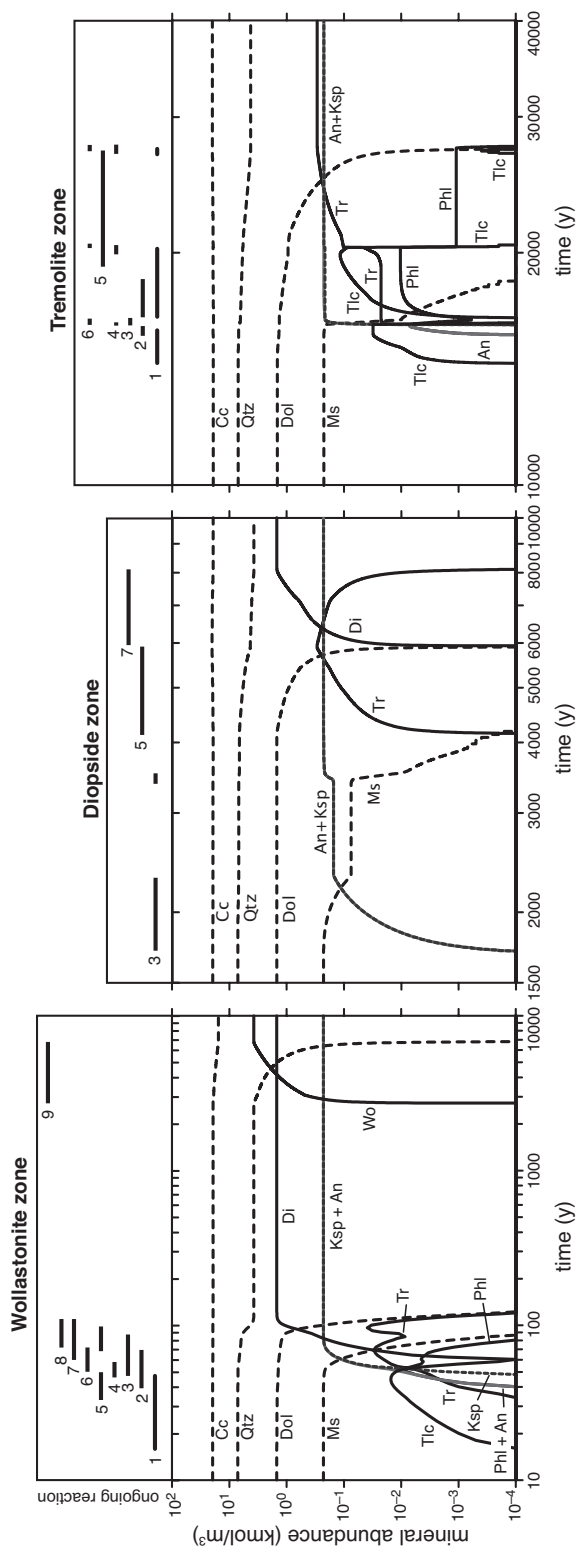

Fig. 8. Reaction progress in selected nodes of wollastonite, diopside, and tremolite zones of traverse B (fig. 1) in model with reaction-enhanced permeability. The shown time periods are different for each node. The nodes are the same for which T-XCO_2^f-t paths are shown in figure 7. Top panels show occurrence of reactions during the simulation. Note that in the diopside and tremolite zones, several reactions are interrupted. Bottom panels show mineral abundances. Abundances of protolith minerals are shown by dashed lines.

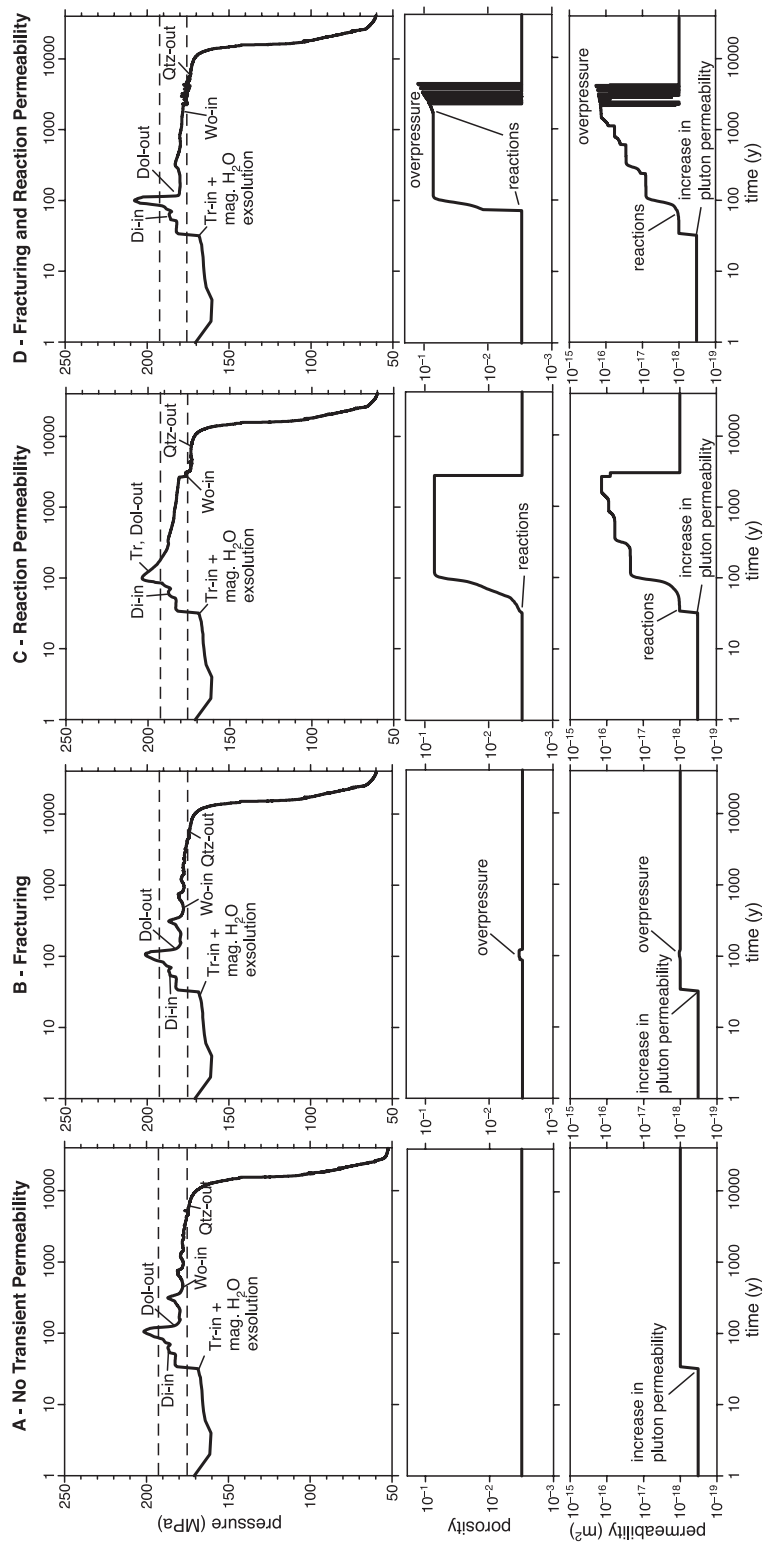

Fig. 9. Evolution of pressure, porosity, and permeability with time in wollastonite-zone node at traverse B (fig. 1) during simulations (A) without transient permeability, (B) with fracturing, (C) with reaction-enhanced permeability, and (D) with both fracturing and reaction-enhanced permeability. The curves are labeled with key occurrences that affect evolution of pressure. Lower dashed line across each of the top panels is lithostatic pressure at this node; the upper dashed line is lithostatic pressure + tensile strength of rocks (15 MPa).

Further away from the contact in the eventual diopside zone, fluid composition initially responds to fluid evolution upstream in the wollastonite zone (figs. 6, 7). The composition becomes CO_2-rich even before the onset of local reactions. Consequently, talc and phlogopite-forming reactions are bypassed. Instead, in the model with reaction-enhanced permeability, the first reaction that occurs is (3), which produces K-feldspar + anorthite (figs. 7, 8). At traverse B, the subsequent reaction is (5), which produces tremolite and consumes dolomite. This reaction ends with the final consumption of dolomite. Diopside is produced by reaction (7) as the fluid composition becomes H_2O-rich, leading to the eventual consumption of tremolite. At traverse A, however, a small amount of diopside is first produced directly from dolomite by reaction (8). The reactions in the diopside zone of course begin later and they are spaced over a longer period than upgrade. Reaction rates range mostly from 10^{-13} to 10^{-11} kmol/m^2/sec, depending on the reaction, the remaining amount of the least abundant mineral, and how far away the actual P-T-$X\mathrm{CO}_2^{\mathrm{f}}$ conditions are from the reaction boundary.

T-$X\mathrm{CO}_2^{\mathrm{f}}$-$t$ paths in the model tremolite zone are characterized by fluctuations in $X\mathrm{CO}_2^{\mathrm{f}}$ during temperature rise and at peak conditions (figs. 6, 7). Production of new minerals can last in excess of 10 k.y., eventually diminishing by 30 ky (fig. 8). The progress of several reactions is interrupted by fluctuations in fluid composition near the temperature maximum. Some reactions occur because they cross stable portions of reaction boundaries, but others occur because they cross metastable extensions of the boundaries. For example, at traverse B with reaction-enhanced permeability, tremolite first appears when the metastable extensions of reactions (4) and (6) are crossed as $X\mathrm{CO}_2^{\mathrm{f}}$ approaches 1. As in the diopside zone, fluid composition is mostly controlled by fluid inflows. Reaction-buffered fluid compositions occur on only small portions of T-$X\mathrm{CO}_2^{\mathrm{f}}$-$t$ paths because the rates of fluid flow usually exceed the reaction rates. The rates of ongoing reactions are typically 10^{-14} to 10^{-12} kmol/m^2/sec.

Pressure, Porosity, and Permeability

Figure 9 shows the evolution of pressure, porosity and permeability in the wollastonite-zone node next to the contact at traverse B during four different simulations—A) without transient permeability, B) with transient permeability related to fracturing, C) with transient permeability related to rock volume decrease with reaction progress, and D) with transient permeability related to both. For the last simulation, subsequent to the initiation of reaction-enhanced permeability, fracturing was allowed to occur when lithostatic pressure only was exceeded. The tensile strength barrier was not applied as it was assumed that once pore space was already expanded once, it is easier to fracture the rock again.

The pressure evolution in all four cases is similar. The first two one-year time-steps are used to equilibrate the model domain, which means that fluid pressure rises close to lithostatic due to the presence of the lithostatically-pressured pluton. Subsequent to the first two time-steps, the pressure slowly rises as the rocks heat-up and the talc-forming reaction is initiated. There is a large jump in pressure in excess of lithostatic at 34 y when fluid exsolution begins in a neighboring node in the pluton. The coincident initiation of tremolite growth plays a subordinate role in the pressure jump. The permeability increase at this time is related to the assumed permeability increase in elements that are shared by nodes of the pluton. Subsequent fluid pressure increase is related to temperature increase and CO_2 production, with the largest pressure increase occurring with progress of the diopside-forming reaction (8), which consumes the largest amount of dolomite. Indeed, in all four simulations the pressure exceeds the lithostatic pressure + tensile strength criterion for fracturing. In the simulation with fracturing, this is exhibited as a small transient increase in porosity and

permeability at about 100 y (fig. 9B). As shown in figure 4, in this model fracturing is predicted to occur only within the first 130 y and in close proximity to the contact.

As the rate of the diopside-forming reaction drops and eventually ceases with diminishing abundance of the rate-controlling dolomite, the pressure also drops but remains above lithostatic for the duration of metamorphism until quartz is eventually consumed by reaction (9). In simulations without reaction-enhanced permeability, the pressure fluctuates in response to ongoing local reactions and pressure changes in neighboring and more distant nodes (figs. 9 A, B). In simulations with reaction-enhanced permeability, the large generated porosity tends to reduce the pressure fluctuations and allow for greater flow-through of fluids because of the greater than 100-fold increase in permeability (figs. 9 C, D). However, once the rate of wollastonite production diminishes as quartz is consumed, fluid pressure drops below lithostatic, which reduces the porosity and permeability. Continued CO_2 production with growth of the remaining wollastonite while pressure is near lithostatic can potentially result in continued transient fracturing which is exhibited by fluctuations in porosity and permeability in figure 9D. Such fracturing may be responsible for the common occurrence of wollastonite along fractures in calc-silicates.

Although there are differences in the details of pressure evolution in the four simulations, the overall similarity is controlled by long-distance pressure gradients in the model domain, from initial high pressures in the pluton to the fixed hydrostatic pressure at the top boundary. Following solidification of the whole pluton at ~25 ky, when fluid pressure in the pluton begins to drop below lithostatic, fluid pressure in the metamorphic aureole is eventually reduced to near hydrostatic by the end of simulations at 40 ky (figs. 5, 9). Localized fracturing seems to have only a small effect on the overall fluid pressure evolution in the model domain, whereas reaction-enhanced permeability moderates pressure fluctuations in the contact aureole.

Fluid Compositions and Fluxes

The evolution of fluid compositions and fluxes is dependent on the exsolution of H_2O from the pluton, generation of CO_2 by metamorphic reactions, and pressure gradients which drive fluid flow. Except for local effects, fracturing and reaction-enhanced permeability have little influence on the overall flow-field in the model domain. Therefore, the broad features of the evolving flow-field can be described by the model without fracturing and reaction-enhanced permeability. The instantaneous flux vectors for 500 y, 10 ky and 40 ky are shown in figure 10, the integrated H_2O and CO_2 fluxes for these times in figure 11, and fluid compositions and densities in figure 12.

The initial flow-field is dominated by CO_2 production in the inner contact aureole and fluid flow away from the lithostatically-pressured pluton toward lower pressures at the margins of the model domain (figs. 10, 11). The instantaneous fluid flux is as much as 2.8×10^{-8} kmol/m^2/sec at the pluton contact when magmatic fluid begins to exsolve out of the pluton. By 10 ky, CO_2 generated in the aureole reaches the top of the model domain, but along the way it is diluted somewhat by H_2O already in the pores (figs. 11, 12). Most H_2O flux is confined to the pluton and the inner aureole, particularly to unreactive beds which do not have high CO_2-dominated fluid pressures. If CO_2 was generated in these beds also, H_2O would be less likely to enter them and most H_2O would be confined to the area of the contact. In effect, while high CO_2 pressures are generated by metamorphic reactions, it is difficult for H_2O to enter the pore space of the pluton's wall rocks. It is only after the rates of CO_2-generating reactions begin to diminish that H_2O can enter the pores and induce the formation of wollastonite. Fluid flow remains generally away from the pluton as long as magmatic H_2O is exsolved at high fluid pressures. However, once the pluton solidifies at ~25 ky, the flow field begins to resemble a Bénard convection with upwelling of CO_2-

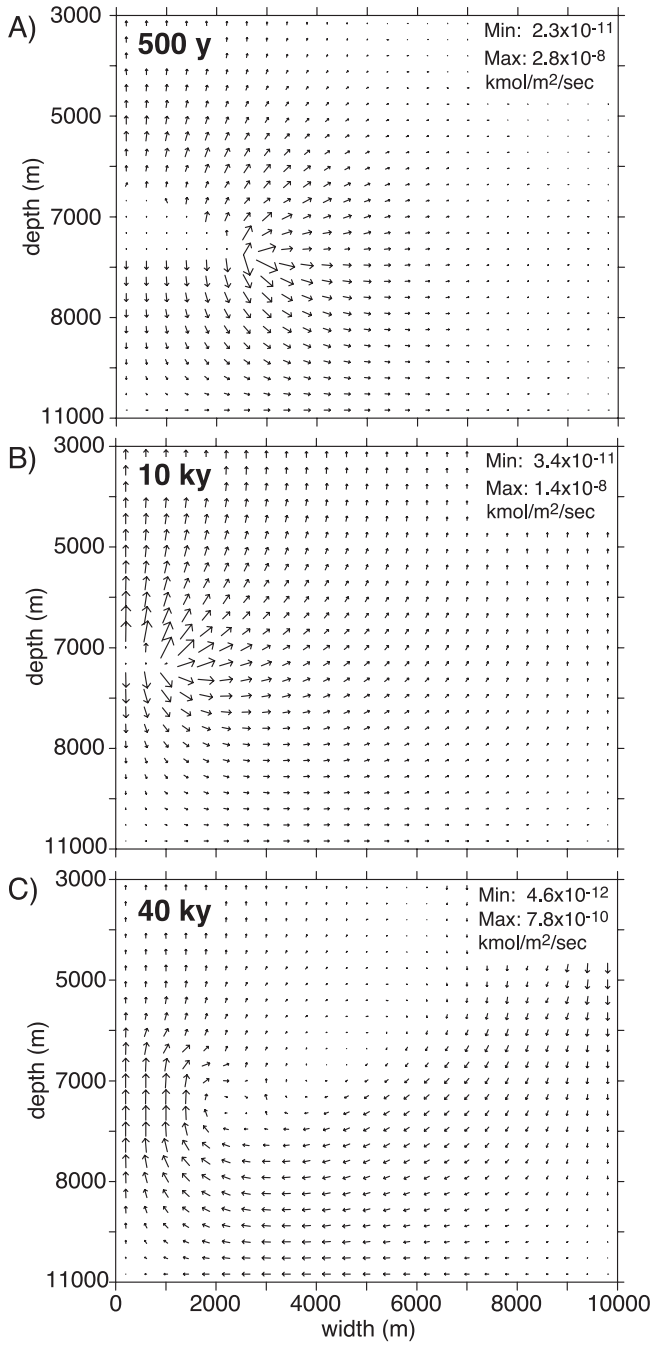

Fig. 10. Flow-field in the model domain at three times after beginning of simulation without transient permeability. The vector field was produced by regridding the dense vector arrays produced in the simulation. Each shown vector represents 8 of the original elements horizontally and 6.4 elements vertically. Lengths of vectors correspond to flux ranges shown in each panel. As long as pluton is exsolving H_2O, fluid flow is generally away from the pluton. Once all of the pluton reaches the solidus, the flow-field resembles Bénard convection. Domain-scale flow-fields for models with transient permeability are not substantially different.

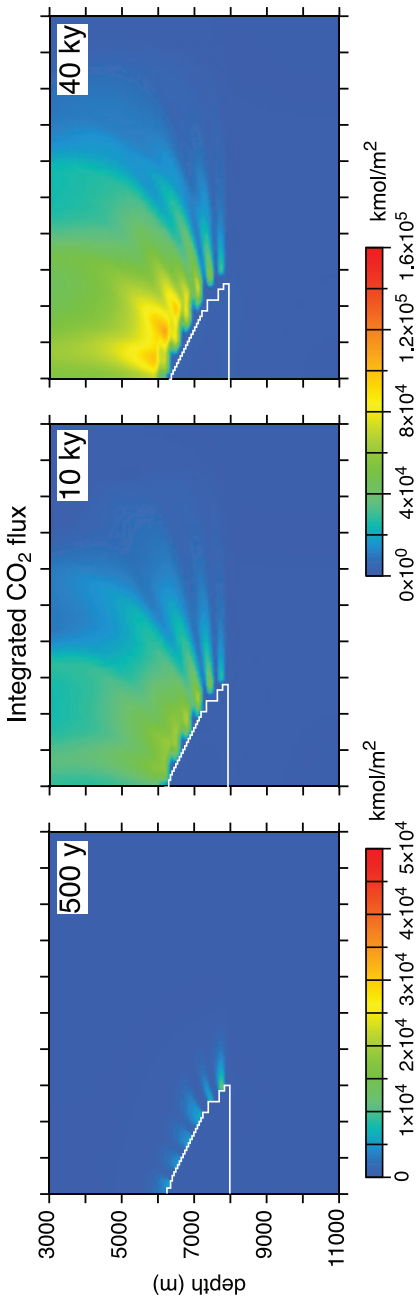

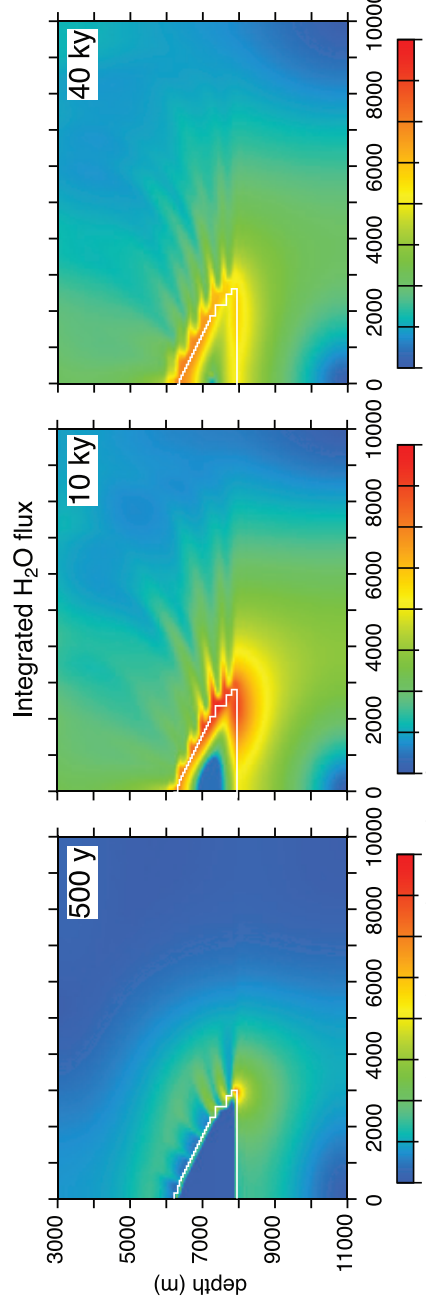

Fig. 11. Integrated CO_2 and H_2O fluxes at three times after beginning of simulation without transient permeability. Domain-scale fluxes for models with transient permeability are not substantially different. The abscissa of each panel is the width of the model domain. All fluxes are given in kmol/m^2. The pluton boundary is outlined for reference.

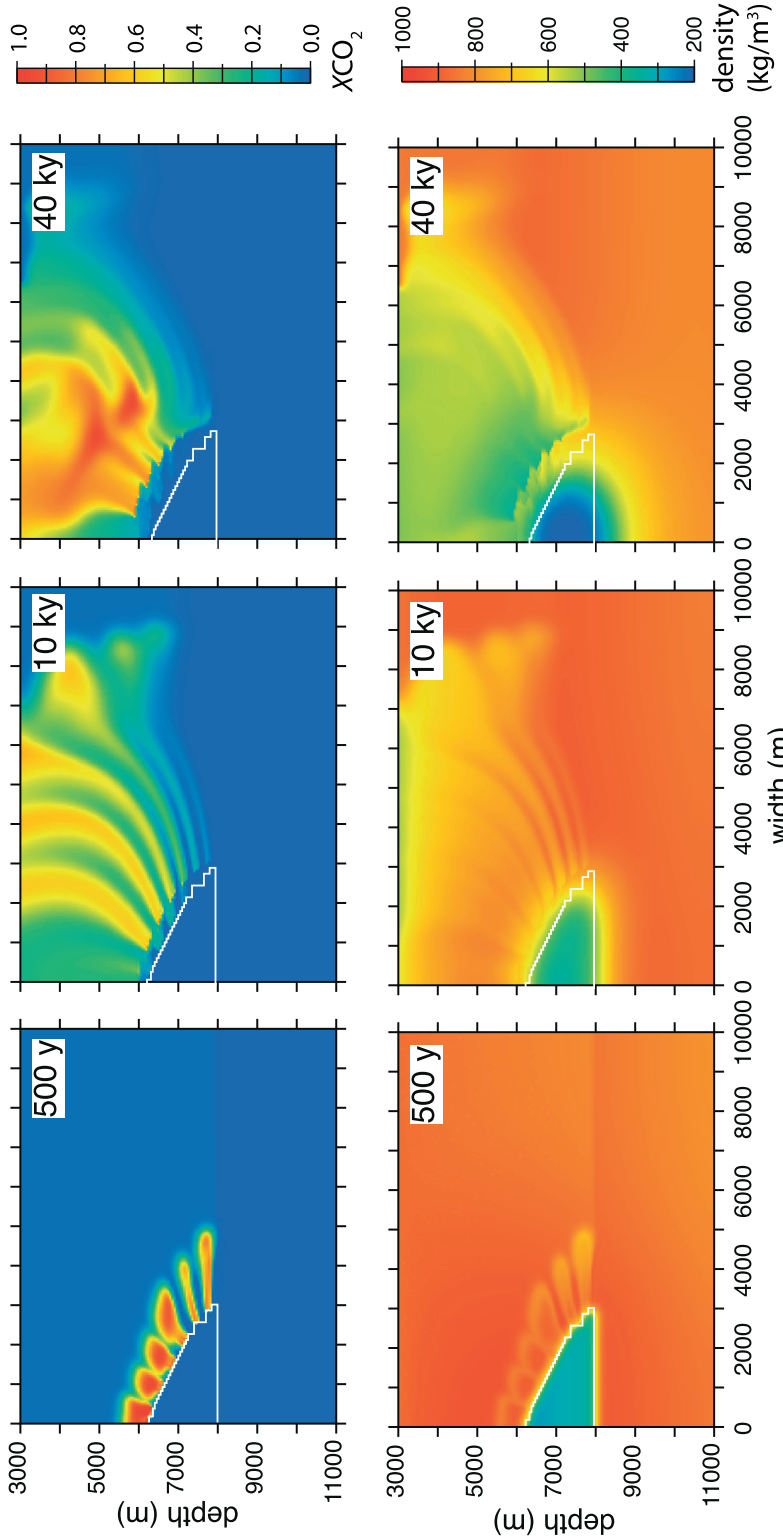

Fig. 12. Fluid compositions (XCO_2^f) and densities at three times after beginning of simulation without transient permeability.

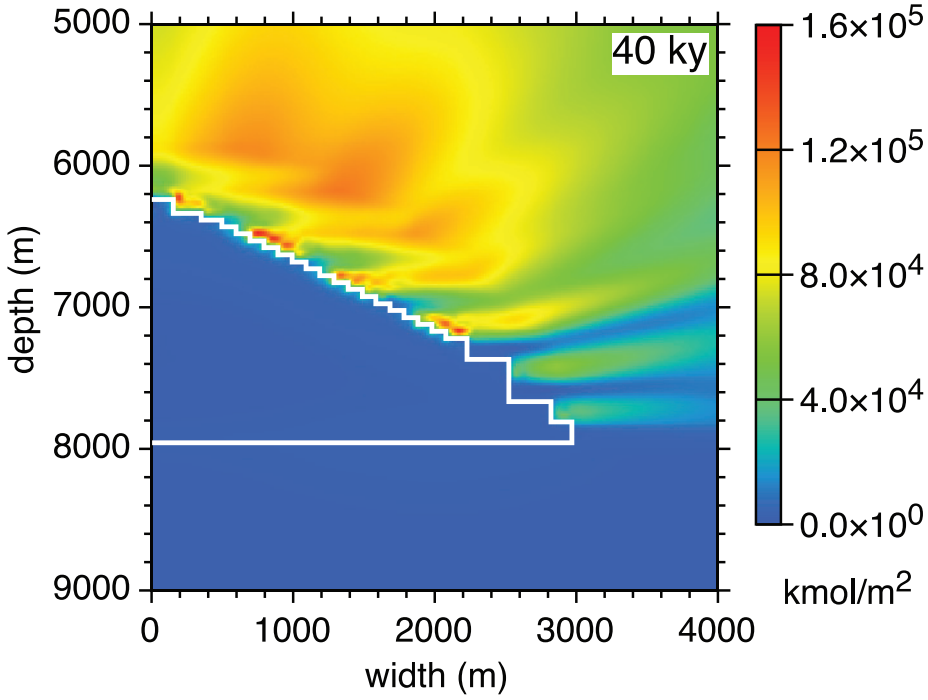

Fig. 13. Close-up of integrated CO_2 flux after 40 ky in the vicinity of the pluton in a model with reaction-enhanced permeability. Nodes that have experienced reaction-enhanced permeability show high CO_2 fluxes in comparison with a model without reaction-enhanced permeability (fig. 11).

dominated fluid above the pluton and downwelling of H_2O-dominated fluid far away from the pluton (fig. 10). By 40 ky, the integrated CO_2 flux is the largest, up to $\sim 1.5 \times 10^5$ kmol/m^2 above the pluton and the H_2O flux is the largest, up to about the same amount in the pluton and its close proximity (fig. 11).

In the reaction-enhanced permeability model, CO_2 that is generated by metamorphic reactions pools in high porosity-permeability regions of the inner aureole (fig. 13), with the consequence that the production of wollastonite occurs later (2700 y) compared to a model with no reaction-enhanced permeability (450 y). Furthermore, reaction-enhanced permeability induces a region of net upward, contact-parallel fluid flow (fig. 14) that is predicted to occur with focusing of flow into high-permeability regions (Yardley and Lloyd, 1995; Ague, 2003). Such contact-parallel flow region is evident in the wollastonite zone at Notch Peak where subvertical flow through unreactive beds between reactive calc-silicates occurred through fractures (Nabelek, 2002). The contact-parallel flow diminishes, however, when pore-space collapses after fluid pressures drop below lithostatic.

Mineral Assemblages

The distribution of model metamorphic mineral assemblages is rather insensitive to transient increases in porosity and permeability in comparison to its dependence on the overall heat and fluid flow in the model domain and the kinetics of the metamorphic reactions. Models that include fracturing and reaction-enhanced permeability yield mineral distributions that are not substantially different from those shown in

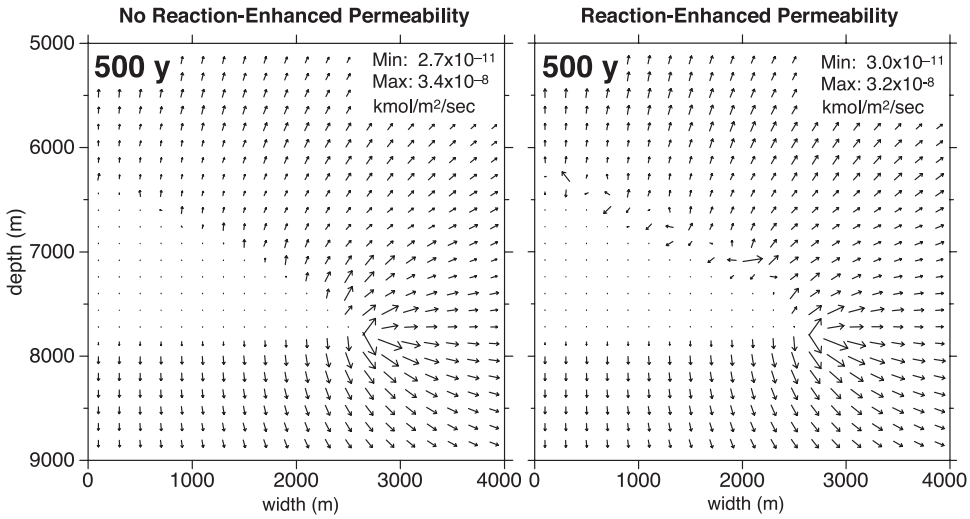

Fig. 14. Close-ups of flux vectors at 500 y in the vicinity of the pluton in models without and with reaction-enhanced permeability. The vector field was produced by regridding the dense vector array produced in the simulations. Each shown vector represents 4 of the original elements horizontally and 3.2 elements vertically. Although flux is dominantly away from the intrusion in the whole model domain, with reaction-enahanced permeability there is localized flow in high-permeability region next to the pluton. Toward the top of the laccolith, the net flow is contact-parallel and upwards.

figure 15. Wollastonite occurs in narrow zones next to the contact in reactive rocks that were eventually infiltrated by magmatic fluid. The wollastonite zone is ~300 m thick in the perpendicular direction from the inclined contact. This thickness corresponds well to the estimated 300 to 350 m thickness of the wollastonite zone in the Notch Peak aureole (Nabelek and Labotka, 1993). The distance of the model diopside isograd is ~600 m, whereas at Notch Peak it is estimated to be at 700 m. The large abundance of model diopside corresponds to the large abundance of diopside in the Notch Peak aureole. The maximum distance of model phlogopite from the contact is ~900 m, whereas at Notch Peak it is estimated to be ~1300 m from the contact. Thus, there appears to be an increasingly larger discrepancy between the model isograd distances and observed distances. However, in the estimate of the perpendicular isograd distances at Notch Peak, it was assumed that the intrusion had a spherical upper contact, such that its dip increased with distance from the contact at the erosion surface. If the contact has a constant dip, then the estimated isograd distances at Notch Peak become closer to the model distances.

As at Notch Peak, the amount of model tremolite is small in comparison with the amount of diopside, and there is also a corresponding overlap in their occurrence. The amount of model phlogopite is smaller than at Notch Peak, which can be explained by the lack of Fe in the model chemical system, as the presence of Fe increases the stability field of biotite at the expense of talc (Nabelek, 2002). Talc was produced in the Fe-absent model system. Talc does not occur at Notch Peak in Fe-bearing rocks, including the Weeks Formation whose mineral assemblages are modeled here, but it occurs in marble beds. In the model, the distribution of anorthite corresponds to the distribution of K-feldspar because their mutual occurrence is determined in the final assemblages by reaction (3), although anorthite can previously be produced by the phlogopite-forming reaction (2). The occurrence of model K-feldspar + anorthite extends beyond the phlogopite and talc isograds because these two minerals are also

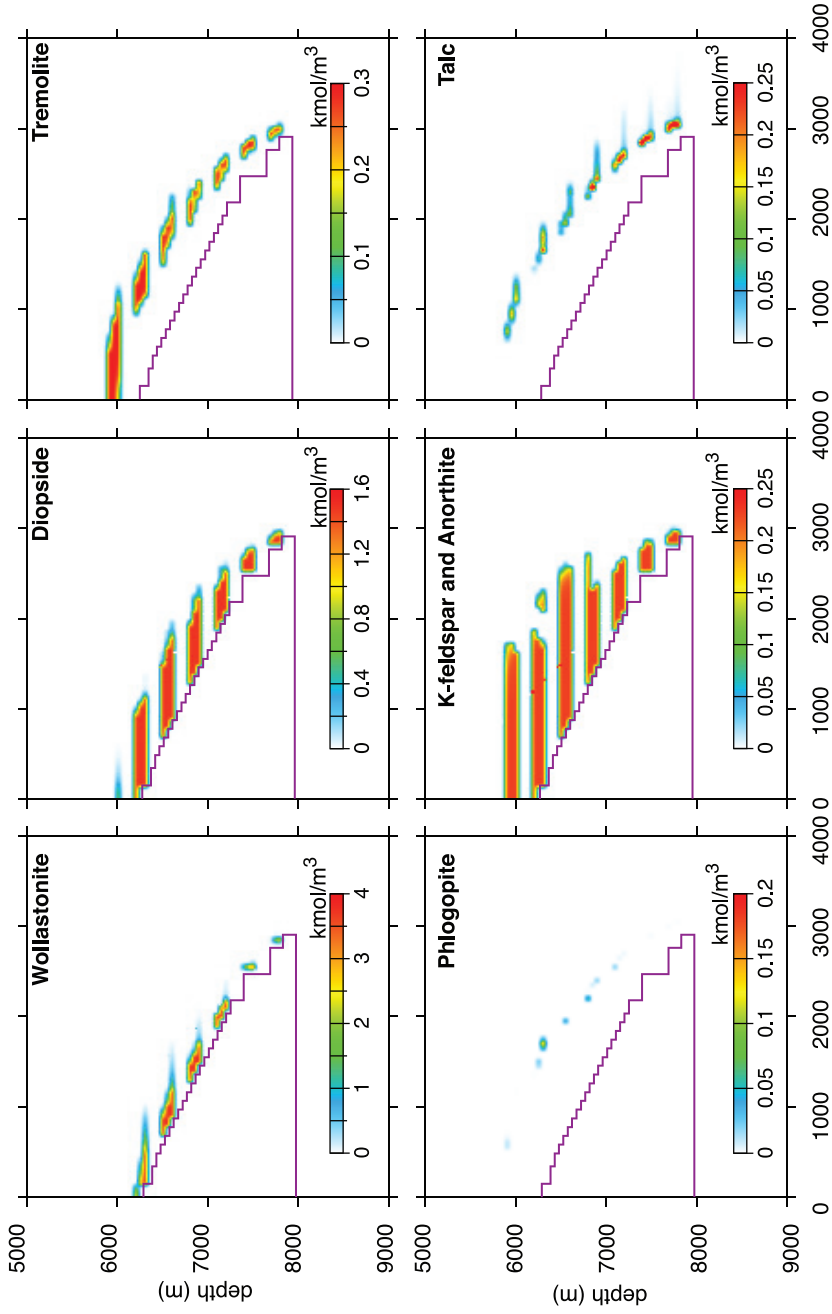

Fig. 15. Calculated abundances of metamorphic minerals (kmol/m^3) after 40 ky in the model contact aureole in simulation without transient permeability. Abundances are not substantially different for models with transient permeability. The pluton boundary is shown for reference. The metamorphic minerals only occur in reactive calc-silicate layers.

produced by infiltration of CO_2 into rocks that are heated above 350°C, as shows by the T-XCO_2-t paths for low-grade rocks (fig. 6). The broad occurrence of K-feldspar + anorthite in the model corresponds to the plume of CO_2 above the intrusion that was generated in higher-grade rocks. It is unknown if such a broad distribution of K-feldspar + anorthite occurs at Notch Peak, but it is worth noting that newly-produced feldspars could be mistaken for detrital feldspars in rocks.

DISCUSSION

The significant overstepping of reactions and delayed consumption of reactant minerals predicted by the models agree with previous predictions that reactions in calc-silicates during rapid heating are likely to be metastable (Bolton and others, 2004; Lüttge and others, 2004). In rocks that have not been infiltrated by fluids from elsewhere prior to the onset of reactions, pore fluid should evolve toward nearly pure CO_2 with reaction progress. Therefore, diopside may be produced directly from dolomite by reaction (8) instead of from tremolite by reaction (7) as the equilibrium path for the modeled rock would predict. Reaction (8) is the sum of reaction (5), which produces tremolite from dolomite, and reaction (7). There is evidence from several contact aureoles that fluid compositions were initially driven to high XCO_2^f because of incomplete reactions. For example, in the Marysville aureole, Montana, Rice (1977) suggested that tremolite was produced by reaction (5) and diopside subsequently on reaction (7) under high XCO_2^f conditions. Rice's (1977) analysis assumed an equilibrium T-XCO_2^f path along reaction boundaries. It is possible, however, that diopside was produced directly from dolomite. Müller and others (2004) used oxygen isotopes to demonstrate that forsterite in the Ubehebe aureole, California, formed directly from metastable dolomite instead of from tremolite or diopside, which are the possible equilibrium reactants.

In the Notch Peak aureole, mineral assemblages in silicate-poor marble beds of the Big Horse Member of the Orr Formation suggest high-XCO_2 fluid compositions, including during the production of tremolite by reaction (5) (Hover-Granath and others, 1983). Nevertheless, in the tremolite zone, the marble beds commonly also contain remnant talc. At higher grades, some forsterite-bearing rocks still contain both diopside and tremolite. In the Weeks Formation there are zones in which tremolite and diopside coexist (Hover-Granath and others, 1983), although at equilibrium they should only coexist on reaction (7). While their coexistence could be interpreted as evidence that fluid composition in these rocks was buffered by the reaction, given the rather high predicted fluid fluxes through the Weeks Formation, it is unlikely that the fluid composition would remain buffered. As suggested by the models, fluid compositions in the diopside and tremolite zones are largely controlled by fluid inflows instead of internal buffering (figs. 6, 7).

The models predict that while exsolution of water out of the pluton and metamorphic reactions in the metamorphic aureole are ongoing, the inner aureole is dominated by magmatic H_2O whereas the outer aureole, especially above the pluton, is dominated by CO_2. CO_2 dominates the pore-space until it is eventually diluted by H_2O initially coming from the crystallizing pluton and later from the Bénard-type convective system. Because the SUTRA code does not permit modeling of two-phase fluid flow, possible differential flow of unmixed CO_2 and H_2O was not modeled. Nevertheless, the models predict that even in relatively high-temperature diopside zones of contact aureoles, fluid unmixing is likely to occur as the fluid composition path crosses the H_2O-CO_2 solvus even before the onset of metamorphic reactions (figs. 3, 6, 7). Various equations of state (Holland and Powell, 1991; Duan and Zhang, 2006) show that within the P-T range of most contact aureoles, H_2O can be more buoyant than CO_2-bearing fluids, but when salts are dissolved in the aqueous phase it can become

denser. If CO_2 is then preferentially removed, it may lead to local H_2O enrichment and a shift in the stable mineral assemblage. For example, although in the models talc is produced in the outer aureole as CO_2 becomes eventually diluted, the common occurrence of talc in outer pars of many dolomitic aureoles, such as Alta, Utah (Moore and Kerrick, 1976) and marble beds at Notch Peak (Hover-Granath and others, 1983), may also be the consequence of preferential removal of CO_2 to produce a fluid that is dominated by H_2O and thus stabilize talc. Preferential removal of CO_2 will also increase the activity of $NaCl_{aq}$ that can eventually result in stabilization of minerals such as scapolite, which is common in calc-silicate aureoles, including Notch Peak.

The models predict high-H_2O fluxes in inner, high-temperature portions of contact aureoles. These zones are characterized by occurrences of wollastonite and vesuvianite in calcite-dominated aureoles (Burnham, 1959; Labotka and others, 1988; Nabelek, 2002), and periclase and brucite in dolomitic aureoles (Moore and Kerrick, 1976; Bowman and Essene, 1982; Ferry and Rumble, 1997; Müller and others, 2009). These inner-aureole zones are typically also characterized by oxygen isotope depletions that point to respective plutons as sources of H_2O that led to production of the mineral assemblages (Nabelek and others, 1984; Nabelek, 1991; Bowman and others, 1994). Nabelek and Labotka (1993) calculated assuming one-dimensional chromatographic exchange that to produce the ~250 m wide zone of oxygen isotope depletion in the wollastonite zone of the Notch Peak aureole, integrated flux of 1.8×10^4 kmol/m^2 of magmatic water was required. This value is in very good agreement with the H_2O flux of 3×10^4 kmol/m^2 required to produce the width of the wollastonite zone by ~20 ky in the current models with or without reaction-enhanced permeability. Similar integrated flux values, ranging from 1.0×10^4 to 4.2×10^4 kmol/m^2 were obtained by Ferry (1994) and Cook and Bowman (2000) to explain the width of the periclase zone in the Alta aureole.

The hot CO_2-rich pore fluid that is produced by metamorphic reactions rises because it is more buoyant than colder H_2O-rich pore fluid that exists in the host rocks far away from the intrusion (fig. 12). Eventually the CO_2 may enter a shallow groundwater system. For example, carbon isotope evidence from several active geothermal systems, including the Larderello and Tyrrhenian systems of Italy (Chiodini and others, 1995; Gianelli and others, 1997; Chiodini and others, 2000), and the Geysers-Clear Lake field of California (Bergfeld and others, 2001a), shows that CO_2 and CH_4 that occur at shallow depths are derived from intrusion-induced metamorphism of calcareous rocks or organic-rich shales. Deep drilling shows that fluid pressures often reach lithostatic conditions and show separation (boiling) of CO_2 from H_2O. By 20 ky, when metamorphism in the model aureole begins to wane, the average CO_2 flux at the top of the model domain is $\sim2.3\times10^3$ mol/m^2/y. This flux is comparable to the measured CO_2 flux of 4.7×10^3 mol/m^2/y in the Dixie Valley geothermal field, Nevada, where the carbon is derived from thermal decarbonation of calcite (Bergfeld and others, 2001b), but it is almost an order of magnitude lower than the measured CO_2 flux of 1×10^4 mol/m^2/y in the Albani Hills volcanic field of Italy, where the source of carbon appears to be heated, buried carbonate formations (Chiodini and Frondini, 2001). CO_2 emissions out of the Albani Hills geothermal field are also punctuated occasionally by anomalously high discharges, and it must be recognized that the amount of emitted CO_2 in a given geothermal field depends on the amount of reactable carbon in rocks that are metamorphosed. Nevertheless, the presented models underscore the potential contribution of metamorphic CO_2 to the budget in the groundwater systems and the atmosphere. In contrast, models with unconstrained pressure at the upper boundary, that is unvented systems for which models were not shown above, point to accumulation of CO_2 in the vicinity of the pluton.

ACKNOWLEDGEMENTS

The author is grateful for constructive reviews by Victor Balashov, Thomas Mueller, Greg Roselle, and the associate editor. James Connolly kindly provided source code for a subroutine to calculate fluid properties. The work was funded by NSF grant EAR-0408564.

References

Ague, J. J., 1995, Deep crustal growth of quartz, kyanite and garnet into large-aperture, fluid-filled fractures, north-eastern Connecticut, USA: Journal of Metamorphic Geology, v. 13, p. 299–314.

——— 2003, Fluid infiltration and transport of major, minor, and trace elements during regional metamorphism of carbonate rocks, Wepawaug Schist, Connecticut, USA: American Journal of Science, v. 303, p. 753–816.

Balashov, V. N., and Yardley, B. W. D., 1998, Modeling metamorphic fluid flow with reaction-compaction-permeability feedbacks: American Journal of Science, v. 298, p. 441–470.

Balashov, V. N., Yardley, B. W. D., and Lebedeva, M. I., 1999, Metamorphism of marbles: Role of feedbacks between reaction, fluid flow, pore pressure, and creep, *in* Jamtveit, B., and Meakin, P., editors, Growth, dissolution, and pattern formation in geosystems: Dordrecht, Kluwer Academic Publishers, p. 367–380.

Baumgartner, L. P., and Ferry, J. M., 1991, A model for coupled fluid-flow and mixed-volatile mineral reactions with applications to regional metamorphism: Contributions to Mineralogy and Petrology, v. 106, p. 273–285.

Bergfeld, D., Geoff, F., and Janik, C. J., 2001a, Carbon isotope systematics and CO_2 sources in The Geysers-Clear Lake region, northern California, USA: Geothermics, v. 30, p. 303–331.

——— 2001b, Elevated carbon dioxide flux at the Dixie Valley geothermal field, Nevada; relations between surface phenomena and the geothermal reservoir: Chemical Geology, v. 177, p. 43–66.

Blencoe, J. G., Seitz, J. C., and Anovitz, L. M., 1999, The CO_2-H_2O system: II. Calculated thermodynamic mixing properties for 400 degrees C, 0–400 MPa: Geochimica et Cosmochimica Acta, v. 63, p. 2,393–2,408.

Bolton, E. W., Rye, D. M., Ague, J. J., and Lüttge, A., 2004, Modeling contact metamorphism of siliceous dolomites via kinetic control of overall reactions: Water-Rock Interactions, v. 11, p. 269–272.

Bowers, T. S., and Helgeson, H. C., 1983, Calculation of the thermodynamic and geochemical consequences of nonideal mixing in the system H_2O-CO_2-NaCl on phase relations in geologic systems—equation of state for H_2O-CO_2-NaCl fluids at high pressures and temperatures: Geochimica et Cosmochimica Acta, v. 47, p. 1,247–1,275.

Bowman, J. R., and Essene, E. J., 1982, P-T-X(CO_2) conditions of contact metamorphism in the Black Butte Aureole, Elkhorn, Montana: American Journal of Science, v. 282, p. 311–340.

Bowman, J. R., Willett, S. D., and Cook, S. J., 1994, Oxygen isotopic transport and exchange during fluid flow: one-dimensional models and applications: American Journal of Science, v. 294, p. 1–55.

Burnham, C. W., 1959, Contact metamorphism of magnesian limesones at Crestmore, California: Geological Society of America Bulletin, v. 70, p. 879–920.

Caciagli, N. C., and Manning, C. E., 2003, The solubility of calcite in water at 6–16 kbar and 500–800 °C: Contributions to Mineralogy and Petrology, v. 146, p. 275–285.

Cathless, L. M., 1981, Fluid flow and genesis of hydrothermal ore deposits: Economic Geology, 75th Anniversary Volume, 424–457.

Chiodini, G., and Frondini, F., 2001, Carbon dioxide degassing from the Albani Hills volcanic region, Central Italy: Chemical Geology, v. 177, p. 67–83.

Chiodini, G., Frondini, F., Cardellini, C., Parello, F., and Peruzzi, L., 2000, Rate of diffuse carbon dioxide Earth degassing estimated from carbon balance of regional aquifers: The case of central Apennine, Italy: Journal of Geophysical Research, v. 105, p. 8,423–8,434.

Chiodini, G., Frondini, F., and Ponziani, F., 1995, Deep structures and carbon dioxide degassing in central Italy: Geothermics, v. 24, p. 81–94.

Cook, S. J., and Bowman, J. R., 2000, Mineralogical Evidence for Fluid-Rock Interaction Accompanying Prograde Contact Metamorphism of Siliceous Dolomites: Alta Stock Aureole, Utah, USA: Journal of Petrology, v. 41, p. 739–757.

Cook, S. J., Bowman, J. R., and Forster, C. B., 1997, Contact metamorphism surrounding the Alta stock: Finite element model simulation of heat- and $^{18}O/^{16}O$ mass-transport during prograde metamorphism: American Journal of Science, v. 297, p. 1–55.

Cui, X., Nabelek, P. I., and Liu, M., 2001, Heat and fluid flow in contact metamorphic aureoles with layered and transient permeability, with application to the Notch Peak aureole, Utah: Journal of Geophysical Research, v. 106, p. 6,477–6,491.

——— 2002, Numerical modeling of fluid flow and oxygen isotope exchange in the Notch Peak contact-metamorphic aureole, Utah: Geological Society of America Bulletin, v. 114, p. 869–882.

——— 2003, Reactive flow of mixed CO_2-H_2O fluid and progress of calc-silicate reactions in contact-metamorphic aureoles: Insights from two-dimensional numerical modeling: Journal of Metamorphic Geology, v. 21, p. 663–684.

Duan, Z., and Zhang, Z., 2006, Equation of state of the H_2O, CO_2, and H_2O-CO_2 systems up to 10 GPa and 2573.15 K: Molecular dynamics simulations with ab initio potential surface: Geochimica et Cosmochimica Acta, v. 70, p. 2,311–2,324.

Dutrow, B., and Norton, D., 1995, Evolution of fluid pressure and fracture propagation during contact metamorphism: Journal of Metamorphic Geology, v. 13, p. 677–686.
Fein, J. B., and Walther, J. V., 1987, Calcite solubility in supercritical CO_2-H_2O fluids: Geochimica et Cosmochimica Acta, v. 51, p. 1,345–1,363.
Ferry, J. M., 1991, Dehydration and decarbonation reactions as a recorder of fluid infiltration: Reviews in Mineralogy, v. 26, p. 351–393.
——— 1994, Role of fluid flow in the contact metamorphism of siliceous dolomitic limestones: American Mineralogist, v. 79, p. 719–736.
Ferry, J. M., and Rumble, D., III, 1997, Formation and destruction of periclase by fluid flow in two contact aureoles: Contributions to Mineralogy and Petrology, v. 128, p. 313–334.
Fuller, E. N., Schettler, P. D., and Giddings, J. D., 1966, A new method for prediction of binary gas diffusion: Industrial and Engineering Chemistry, v. 58, p. 18–27.
Gerdes, M., Baumgartner, L. P., and Person, M., 1998, Convective fluid flow through heterogeneous country rocks during contact metamorphism: Journal of Geophysical Research, v. 103, p. 23,983–24,003.
Gianelli, G., Ruggieri, G., and Mussi, M., 1997, Isotopic and fluid inclusion study of hydrothermal and metamorphic carbonates in the Larderello geothermal field and surrounding areas, Italy: Geothermics, v. 26, p. 393–417.
Greenwood, H. J., 1975, Buffering of pore fluids by metamorphic reactions: American Journal of Science, v. 275, p. 573–593.
Hintze, L. F., 1974, Preliminary geologic map of the Notch Peak quadrangle, Millard Country, Utah.: U.S. Geological Survey Miscellaneous Field Studies.
Holland, T., and Powell, R., 1991, A Compensated-Redlich-Kwong (CORK) equation for volumes and fugacities of CO_2 and H_2O in the range 1 bar to 50 kbar and 100–600°C: Contributions to Mineralogy and Petrology, v. 109, p. 265–273.
——— 1998, An internally consistent thermodynamic data set for phases of petrological interest: Journal of Metamorphic Geology, v. 16, p. 309–343.
Holtz, F., Behrens, H., Dingwell, D. B., and Johannes, W., 1995, Water solubility in haplogranite melts: Compositional, pressure and temperature dependence: American Mineralogist, v. 80, p. 94–108.
Hover-Granath, V. C., Papike, J. J., and Labotka, T. C., 1983, The Notch Peak contact metamorphic aureole: Petrology of the Big Horse limestone member of the Orr Formation: Geological Society of America Bulletin, v. 94, p. 889–906.
Jamtveit, B., Bucher, N. K., and Stijfhoorn, D. E., 1992, Contact metamorphism of layered shale-carbonate sequences in the Oslo Rift; I, Buffering, infiltration, and the mechanisms of mass transport: Journal of Petrology, v. 33, p. 377–422.
Johannes, W., and Holtz, F., 1996, Petrogenesis and Experimental Petrology of Granitic Rocks: Berlin, Springer-Verlag, 335 p.
Labotka, T. C., Nabelek, P. I., and Papike, J. J., 1988, Fluid infiltration through the Big Horse Limestone in the Notch Peak contact-metamorphic aureole, Utah: American Mineralogist, v. 73, p. 1,302–1,324.
Labotka, T. C., Anovitz, L. M., and Blencoe, J. G., 2002, Pore pressure during metamorphism of carbonate rock; effect of volumetric properties of H_2O-CO_2 mixtures: Contributions to Mineralogy and Petrology, v. 144, p. 305–313.
Lasaga, A. C., and Rye, D. M., 1993, Fluid flow and chemical reaction kinetics in metamorphic systems: American Journal of Science, v. 293, p. 361–404.
Lasaga, A. C., Lüttge, A., Rye, D. M., and Bolton, E. W., 2000, Dynamic treatment of invariant and univariant reactions in metamorphic systems: American Journal of Science, v. 300, p. 173–221.
Lockner, D. A., 1995, Rock failure, *in* Ahrens, T. J., editor, Rock physics and phase relations: Washington, D.C., American Geophysical Union, p. 127–147.
Lüttge, A., Bolton, E. W., and Rye, D. M., 2004, A kinetic model of metamorphism: an application to siliceous dolomites: Contributions to Mineralogy and Petrology, v. 146, p. 546–565.
Manning, C. E., and Bird, D. K., 1991, Porosity evolution and fluid flow in the basalts of the Skaergaard magma-hydrothermal system, east Greenland: American Journal of Science, v. 291, p. 201–257.
Manning, C. E., and Ingebritsen, S. E., 1999, Permeability of the continental crust; implications of geothermal data and metamorphic systems: Reviews of Geophysics, v. 37, p. 127–150.
Moore, J. N., and Kerrick, D. M., 1976, Equilibria in siliceous dolomites of the Alta aureole, Utah: American Journal of Science, v. 276, p. 502–524.
Müller, T., Baumgartner, L., Foster, C. T., Jr., and Vennemann, T. W., 2004, Metastable prograde mineral reactions in contact aureoles: Geology, v. 32, p. 821–824.
Müller, T., Baumgartner, L. P., Foster, C. T., Jr., and Bowman, J. R., 2009, Crystal size distribution of periclase in contact metamorphic dolomite marbles from the southern Adamello Massif, Italy: Journal of Petrology, v. 50, p. 451–465.
Nabelek, P. I., 1991, Stable Isotope Monitors: Reviews in Mineralogy, v. 26, p. 395–435.
——— 2002, Calc-silicate reactions and bedding-controlled isotopic exchange in the Notch Peak aureole, Utah: Implications for differential fluid fluxes with metamorphic grade: Journal of Metamorphic Geology, v. 20, p. 429–440.
——— 2007, Fluid evolution and kinetics of metamorphic reactions in calc-silicate contact aureoles—From H_2O to CO_2 and back: Geology, v. 35, p. 927–930.
Nabelek, P. I., and Labotka, T. C., 1993, Implications of geochemical fronts in the Notch Peak contact metamorphic aureole, Utah, USA: Earth and Planetary Science Letters, v. 119, p. 539–559.

Nabelek, P. I., Labotka, T. C., O'Neil, J. R., and Papike, J. J., 1984, Contrasting fluid/rock interaction between the Notch Peak granitic intrusion and argillites and limestones in western Utah: Evidence from stable isotopes and phase assemblages: Contributions to Mineralogy and Petrology, v. 86, p. 25–34.

Nabelek, P. I., Labotka, T. C., and Russ-Nabelek, C., 1992, Stable isotope evidence for the role of diffusion, infiltration and local structure on contact metamorphism of calc-silicate rocks at Notch Peak, Utah.: Journal of Petrology, v. 33, p. 557–583.

Norton, D. L., 1984, Theory of Hydrothermal Systems: Annual Review of Earth and Planetary Sciences, v. 12, p. 155–177.

Oliver, N. H. S., Cartwright, I., Wall, V. J., and Golding, S. D., 1993, The stable isotope signature of kilometre-scale fracture-dominated metamorphic fluid pathways, Mary Kathleen, Australia: Journal of Metamorphic Geology, v. 11, p. 705–720.

Rice, J. M., 1977, Progressive metamorphism of impure dolomitic limestone in the Marysville aureole, Montana: American Journal of Science, v. 277, p. 1–24.

Roselle, G. T., Baumgartner, L. P., and Valley, J. W., 1999, Stable isotope evidence of heterogeneous fluid infiltration at the Ubehebe Peak contact aureole, Death Valley National Park, California: American Journal of Science, v. 299, p. 93–138.

Rumble, D., III., Ferry, J. M., Hoering, T. C., and Boucot, A. J., 1982, Fluid flow during metamorphism at the Beaver Brook Fossil Locality, New Hampshire: American Journal of Science, v. 282, p. 886–919.

Seager, M. K., 1989, A SLAP for the Masses: in Parallel Supercomputing, *in* Carey, G. F., editor, Methods, Algorithms and Applications: New York, Wiley, p. 135–155.

Seitz, J. C., and Blencoe, J. G., 1999, The CO_2-H_2O system. I. Experimental determination of volumetric properties at 400°C, 10–100 MPa: Geochimica et Cosmochimica Acta, v. 63, p. 1,559–1,569.

Shampine, L. F., and Gordon, M. K., 1975, Computer solution of ordinary differential solutions—the initial value problem: San Francisco, W. H. Freeman, 318 p.

Sterner, S. M., and Bodnar, R. J., 1991, Synthetic fluid inclusions. X: Experimental determination of P-V-T-X properties in the CO_2-H_2O system to 6 Kb and 700°C: American Journal of Science, v. 291, p. 1–54.

Takenouchi, S., and Kennedy, G., 1964, The binary system H_2O-CO_2 at high temperatures and pressures: American Journal of Science, v. 262, p. 1,055–1,074.

Voss, C. I., 1984, A finite-element simulation model for saturated-unsaturated, fluid-density-dependent ground water flow with energy transport on chemically-reactive single-species solute transport: U.S. Geological Survey Water Resources Investigations Report, 84-4369.

Voss, C. I., and Provost, A. M., 2002, A Model for saturated-unsaturated, variable-density ground-water flow with solute or energy transport: U.S. Geological Survey Water Resources Investigations Report, 02-4231.

Walder, J., and Nur, A., 1984, Porosity reduction and crustal pore pressure development: Journal of Geophysical Research, v. 89, p. 11,539–11,584.

Yardley, B. W. D., 1986, Fluid migration and veining in the Connemara Schists, Ireland, *in* Walther, J. V., and Wood, B. J., editors, Fluid-rock interactions during metamorphism: New York, Springer-Verlag, p. 109–131.

Yardley, B. W. D., and Lloyd, G. E., 1995, Why metasomatic fronts are really metasomatic sides: Geology, v. 23, p. 53–56.